Fast mechanisms linking the Labrador Sea with subtropical Atlantic overturning

Yavor Kostov[1] · Marie-José Messias[1] · Herlé Mercier[2] · Helen L. Johnson[3] · David P. Marshall[4]

Abstract

We use an ocean general circulation model and its adjoint to analyze the causal chain linking sea surface buoyancy anomalies in the Labrador Sea to variability in the deep branch of the Atlantic meridional overturning circulation (AMOC) on inter-annual timescales. Our study highlights the importance of the North Atlantic Current (NAC) for the north-to-south connectivity in the AMOC and for the meridional transport of Lower North Atlantic Deep Water (LNADW). We identify two mechanisms that allow the Labrador Sea to impact velocities in the LNADW layer. The first mechanism involves a passive advection of surface buoyancy anomalies from the Labrador Sea towards the eastern subpolar gyre by the background NAC. The second mechanism plays a dominant role and involves a dynamical response of the NAC to surface density anomalies originating in the Labrador Sea; the NAC adjustment modifies the northward transport of salt and heat and exerts a strong positive feedback, amplifying the upper ocean buoyancy anomalies. The two mechanisms spin up/down the subpolar gyre on a timescale of years, while boundary trapped waves rapidly communicate this signal to the subtropics and trigger an adjustment of LNADW transport on a timescale of months. The NAC and the eastern subpolar gyre play an essential role in both mechanisms linking the Labrador Sea with LNADW transport variability and the subtropical AMOC. We thus reconcile two apparently contradictory paradigms about AMOC connectivity: (1) Labrador Sea buoyancy anomalies drive AMOC variability; (2) water mass transformation is largest in the eastern subpolar gyre.

Keywords AMOC · Labrador Sea · LNADW · Lower North Atlantic Deep Water · Atlantic Meridional Overturning Circulation · NAC · North Atlantic Current · Surface heat fluxes · Water mass transformation · OSNAP · RAPID-MOCHA

1 Introduction

The Atlantic Meridional Overturning Circulation (AMOC) is an essential part of the climate system as it carries warm water from the tropics northwards and a cold return flow southwards in the deep ocean (Lozier 2012). Recent observations (Li et al. 2021), reanalysis, and modeling-based studies (Zou et al. 2019), have highlighted a gap in the understanding of the latitudinal coherence or the so-called meridional connectivity of the AMOC between the subpolar and subtropical North Atlantic. In particular, there are unanswered questions about the exact role of the Labrador Sea in driving AMOC variability such as the 2004–2012 decline in the RAPID-AMOC at 26°N (Smeed et al. 2014), that was particularly pronounced in the LNADW layer.

A number of studies (e.g., Thornalley et al. 2018) have suggested a connectivity between density anomalies in the Labrador Sea and the strength of the Deep Western Boundary Current (DWBC) in the subtropics. Many studies emphasize the remote impact of the Labrador Sea on long-term buoyancy-driven variability of the subtropical Atlantic meridional overturning circulation (e.g., Eden and Willebrand 2001; Bailey et al. 2005; Getzlaff et al. 2005; Böning et al. 2006; Danabasoglu et al. 2012, Robson et al. 2014; Yeager et al. 2021). On the other hand, on interannual timescales the meridional connectivity between the North Atlantic subpolar gyre (Fig. 1) and the low latitudes is found in the Lower North Atlantic Deep Water (LNADW) (Zou et al. 2019; Frajka-Williams et al. 2016; McCarthy et al. 2012; Smeed et al. 2014), a dense

✉ Yavor Kostov
y.kostov@exeter.ac.uk

1   University of Exeter, Geography, Exeter, UK

2   University of Brest, Laboratoire d'Océanographie Physique et Spatiale, CNRS, Brest, France

3   University of Oxford, Earth Sciences, Oxford, UK

4   University of Oxford, Physics, Oxford, UK

Fig. 1 Climatology of the relative dynamical sea-surface height [m] in ECCO. We use sea surface height to distinguish the subtropical gyre (positive values in yellow, orange, and red) from the subpolar and the northern recirculation gyres (negative values in blue)
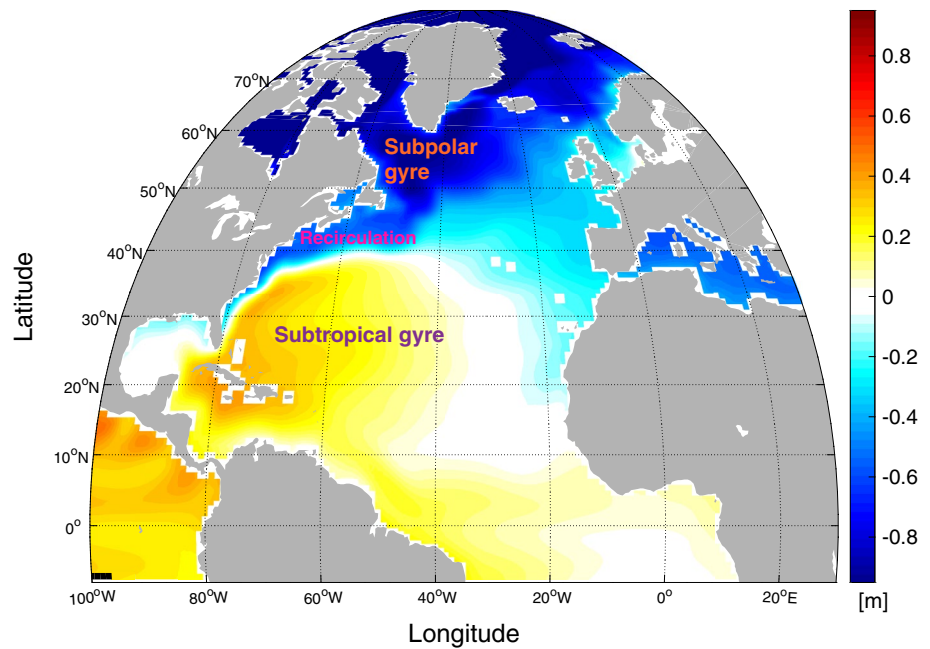
water mass that is not formed and normally not ventilated in the Labrador Sea but is instead the product of overflow waters entering the Atlantic basin further north-east. In addition, there is substantial observational evidence that water mass transformation in the eastern subpolar gyre plays a more important role both for the time-mean climatological AMOC and its variability Lozier et al. (2019); Desbruyeres et al. (2019); Petit et al. (2020)] compared to the Labrador Sea. Thus Lozier et al. (2019) suggest that the apparent connectivity between the Labrador Sea and the subtropical AMOC is possible if: (1) Labrador Sea density anomalies are signatures of density anomalies imported from the eastern subpolar gyre (Menary et al. 2020), where LNADW constituents originate; and/or (2) Labrador Sea density anomalies exert a remote impact on water mass transformation in the eastern subpolar gyre.

Here we use the MITgcm ocean general circulation model and its adjoint (Marshall et al 1997; Marotzke et al 1999) to show that there is indeed an oceanic teleconnection between the Labrador Sea and the eastern subpolar gyre. This teleconnection modifies the southward transport of LNADW all the way to the subtropics. To illustrate this connectivity, we focus on the sensitivity of transports across key vertical sections in the North Atlantic to surface boundary conditions in the subpolar gyre (Fig. 2). We restrict our attention to the linear regime by deliberately considering small forcing anomalies. We identify two causal pathways that link Labrador Sea density anomalies to variability in the subtropical overturning: (1) an advection of the original upper ocean Labrador Sea buoyancy anomalies by the background circulation; and (2) a concurrent adjustment of the NAC that modifies northward salt transport and surface heat fluxes over the subpolar gyre.

The North Atlantic Current (NAC) plays a central role in both mechanisms that we identify in our model-based experiments.

Once the currents in the eastern subpolar gyre adjust in response to Labrador Sea density anomalies, coastally-trapped waves communicate this signal along the boundary from Greenland to the subtropics. In this sense, our results build upon the paradigm of Zhang (2010) who suggests two regimes of north–south connectivity in the AMOC: a slow (3-to-4-year) southward advection of anomalies in the subpolar gyre north of 35°N and a fast (< 1 month) wave adjustment in the lower latitudes. In our study, we suggest that the characteristic timescale of the slow subpolar regime is set by *north-eastward* advection of upper ocean density anomalies along the NAC rather than direct southward advection along the deep western boundary current (DWBC).

In Sect. 2, we describe the setup of our numerical model. In Sect. 3, we present evidence of a causal connection between the western Labrador Sea, water mass transformation in the eastern subpolar gyre, the subtropical overturning, and the southward export of LNADW. Section 4 demonstrates a meridionally coherent velocity anomaly in LNADW in response to surface freshening along the western boundary of the Labrador Sea. Section 5 highlights the importance of positive feedback mechanisms that amplify upper ocean density anomalies originating in the western Labrador Sea. In Sect. 6, we explore the elements of the causal chain linking the Labrador Sea with subtropical overturning on fast timescales. In Sect. 7, we consider recent historical variability in the North Atlantic and relate it to the mechanisms that we identify in our study. In Sect. 8, we discuss our results and the implications of our study.
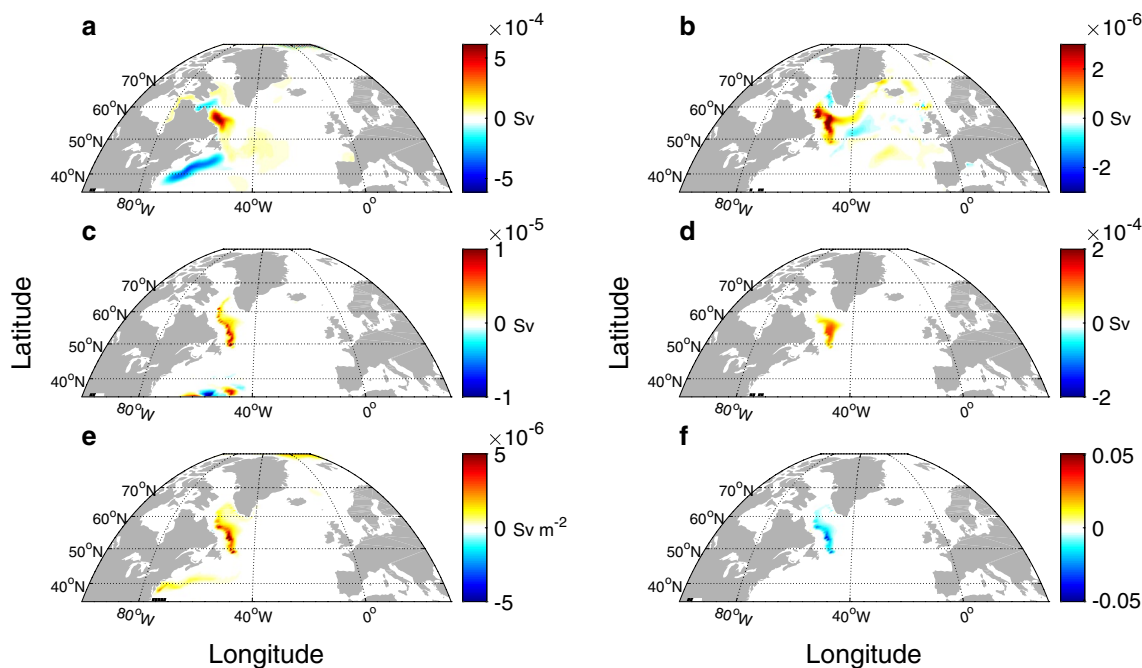
Fig. 2 Sensitivity [Sv/ (dimensionless SSS anomaly sustained over 1 h)] of **a** the winter NAC volume transport at 45°N to SSS at a lead time of 200 days (Adjoint experiment A1_NAC, Table 1 in Appendix); **b** the spring OSNAP-East overturning to SSS [Sv per dimensionless SSS change] at a lead time of 2 years (Adjoint experiment A2_OSNAPE, Table 1 in Appendix; **c** the winter-time southward DWBC transport at 26° N in the σ_θ range 27.81–27.86 [kg m^{-3}] to SSS [Sv per dimensionless SSS change] at a lead time of approximately 4 years (Adjoint experiment A3_DWBC26°N, Table 1 in Appendix). The DWBC cost function at 26° N was computed west of 70°W in a density layer corresponding to LNADW components;

d sensitivity of the winter RAPID-MOCHA overturning at 26° N to SSS [Sv per dimensionless SSS change] at a lead time of approximately 4 years (Adjoint experiment A4_AMOC26° N, Table A1, and Kostov et al. 2021). **e** Contribution of SSS variability to historical intermonthly variability of the RAPID-MOCHA AMOC in ECCO [Sv m^{-2}], estimated by projecting SSS variability onto the adjoint sensitivity patterns (Kostov et al. 2021) of the RAPID-MOCHA AMOC to SSS (e.g., the sensitivity pattern shown in **d**). Panels a through e are based on output from the adjoint of the MITgcm; **f** SSS perturbation applied to the Labrador Sea motivated by the results in **d**, **e**

2 Methods

We use the state-of-the-art MITgcm ocean circulation model (Marshall et al. 1997) in the ECCO state estimate configuration (Marotzke et al. 1999; Forget et al. 2015a, b; Pillar et al. 2016; Smith and Heimbach 2019; Fukumori et al 2017, 2018) with a nominal 1×1 degree resolution on a latitude-longitude-cap grid. ECCO is an ocean state estimate (Forget et al. 2015a) in which the ocean model is fit to observations and skillfully reproduces the evolution of historical ocean properties (Jackson et al. 2019; Kostov et al. 2021), while remaining dynamically consistent.

We use algorithmic differentiation software (TAF, Giering 2010), to obtain the adjoint of the MITgcm (Marotzke et al. 1999; Pillar et al. 2016; Smith and Heimbach. 2019). To investigate the meridional AMOC connectivity, we define several quantities of interest (Table 1 in Appendix, adjoint experiments 1–4) including the monthly-averaged overturning across 26° N (in depth space) and across the OSNAP-EAST line (in σ_θ coordinates, which better reflect the rate of subpolar

water mass transformation compared to z-coordinates (Lherminier et al. 2007 and Lozier et al. 2019). We also consider the northward NAC transport across 45° N (See Fig. S1 in the Supplementary Information) as a separate quantity of interest. The adjoint allows us to calculate the lagged sensitivity of these transport metrics to surface boundary conditions including sea-surface temperature and salinity (SST and SSS; See Fig. 2). For example, we obtain the sensitivity of northward transport by the NAC at 45° N, V_{NAC}, to SSS at each geographical location **x** at lead time τ:

$$\frac{\partial}{\partial} \frac{V_{NAC}}{SSS(\boldsymbol{x}, \tau)}, \tag{1}$$

and similarly for the other quantities of interest that we consider, such as the AMOC at 26° N, Ψ_{26N}.

The sensitivity patterns obtained from the adjoint model calculation motivate a set of forward perturbation experiments in the ECCO configuration (Table 1 in Appendix, experiment Pert1_LabSSS) whereby we instantaneously decrease the SSS in the western Labrador Sea. Similarly, we apply a passive

tracer anomaly that mimics the SSS perturbation (Table 1 in Appendix, experiment Pert2_LabPtrac). We thus attempt to understand the causal pathways that link events such as the 2004–2012 decline in subtropical LNADW transport (Smeed et al. 2014) to the Labrador Sea, as suggested by Kostov et al. (2021). We choose to perturb surface salinity rather than temperature because SST anomalies have a shorter timescale of persistence due to air-sea heat exchange (Kostov et al. 2019), which is parameterized in this model configuration. We deliberately apply very small SSS perturbations to ensure that the response remains in the linear regime.

3 Causal connectivity between the Labrador Sea surface and the subtropical AMOC

The adjoint of the MITgcm (Marotzke et al. 1999; Pillar et al. 2016; Smith and Heimbach 2019) outputs sensitivity maps that allow us to demonstrate the existence of causal links between Labrador Sea surface buoyancy anomalies and volume transport in other parts of the Atlantic Ocean (Fig. 2). First, we find that the NAC transport across 45°N is particularly sensitive to surface salinity anomalies near the southwestern boundary of the Labrador Sea at a lead-time of 6 months to 1 year (Fig. 2a). In Sect. 6, we show that this sensitivity is related to the southward transport of density anomalies along the Labrador Current and ultimately to changes in the geostrophic balance at the point where the NAC crosses 45° N, the so-called mid-latitude "transition zone" (Buckley and Marshall 2016).

We also find that on annual and interannual timescales, the overturning across OSNAP-EAST, the southward DWBC transport at 26° N in the σ_θ range 27.81–27.86, and the AMOC across 26°N are similarly sensitive to surface density anomalies in the western Labrador Sea (Fig. 2b–d). The overturning sensitivity to surface buoyancy anomalies in the Labrador Sea is not a purely hypothetical construct because the ECCO state estimate shows that there is strong surface SSS variability that activates these sensitivity patterns (Fig. 2d and Kostov et al. (2021)). Similar results as in Fig. 2a–d but with different magnitudes are obtained for other seasons (not shown). Both the AMOC sensitivity (Fig. 2d) and the projection of SSS variability on the AMOC sensitivity patterns (Fig. 2e) are particularly pronounced in the western part of the basin (Kostov et al. 2021). This region has been identified by MacGilchrist et al. (2020), Georgiou et al. (2020), and Desbruyeres et al. (2021) as important for boundary current subduction and ocean ventilation.

If large winter mixed layer depth were the decisive factor for meridional connectivity on fast timescales, then the convective interior of the basin would be at least as important as the boundary (Extended Data Fig. 5 in Kostov et al. (2021)). Instead, our results point to a mechanism connecting western boundary density anomalies in the Labrador Sea with the rate of subtropical overturning. These results force us to consider processes that impact AMOC variability on short timescales but are not driven by deep convection in the interior of the Labrador Sea (See discussion in Kostov et al. (2021)).

4 Meridional coherence

We explore the meridional connectivity between the subpolar and subtropical gyre. To that end, we apply an initial condition SSS perturbation in the western Labrador Sea (Pert1_Lab-SSS in Table 1 in Appendix) in January 1996 of the ECCO state estimate (Ctrl1_ECCO in Table 1 in Appendix). The spatial structure of the perturbation (Fig. 2f) is based on and motivated by the projection of SSS variability on the AMOC sensitivity patterns (Fig. 2d and e, and Kostov et al. (2021)). We perturb only the ocean surface, but the imposed anomaly spreads vertically within the mixed layer. The magnitude of the imposed freshening anomaly SSS_{anom} is deliberately very small in order to explore the response of the overturning in a linear regime. Hence, based on the adjoint sensitivity maps, we expect a very small AMOC response in the subtropics Ψ_{26N} on the order of 10^{-5} to 10^{-4} Sv. Our goal is to identify causal mechanisms rather than generate a significant AMOC anomaly.

In response to the imposed Labrador Sea freshening, the rates of overturning at the OSNAP-EAST and the RAPID arrays decline (Fig. 3) in agreement with our expectations based on the adjoint (Fig. 2b–d). Both OSNAP-EAST overturning and the subtropical AMOC show an initial response within a year after the perturbation. However, the adjustment timescale at OSNAP-EAST is approximately 2 years (Fig. 3), the timescale on which surface fluxes over the Iceland Basin respond to the Labrador Sea freshening (Sect. 6b and Figs. 14 and 15). In comparison, the subtropical AMOC takes ~4 years to adjust (Fig. 3), the timescale on which density anomalies and sea surface height anomalies reach Southern Greenland (Fig. 4).

Figure 5b, c shows the vertical structure of the resulting velocity anomaly at 26°N in the Labrador Sea freshening experiment Pert1_LabSSS (Table 1 in Appendix) once the subtropical overturning has already responded, by Year 5. While the climatological lower AMOC branch at 26°N is strongest in the Upper North Atlantic Deep Water (UNADW) layer (Fig. 5a) which contains exported Labrador Sea Water (Zou et al. 2019), the DWBC transport anomaly in response to Labrador Sea freshening spans both the UNADW and the LNADW layers (Fig. 5b). In fact, the "bull's eye" of the deep AMOC response at 26°N lies between σ_θ of 27.81 and 27.86 [kg m^{-3}] (Fig. 5c). In the Labrador Sea, as represented in this model configuration, σ_θ of 27.81 to 27.86 [kg m^{-3}] corresponds to North East Atlantic Deep Water (NEADW).

Fig. 3 Anomaly in the OSNAP-EAST overturning (at approximately 57 °N–60° N) and the RAPID-AMOC at 26° N in response to the Labrador Sea freshening applied as an initial condition perturbation in January 1996 (experiment Pert1_LabSSS). The OSNAP-EAST timeseries is filtered using a method based on median absolute deviations (MAD) to remove several peaks due to noise. These peaks are amplified as a result of remapping into density space. Ticks along the horizontal axis mark the beginning of each year
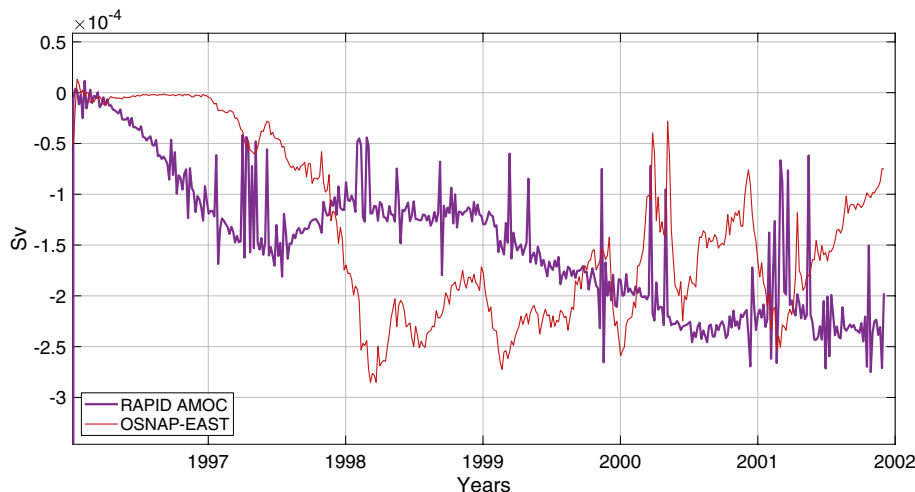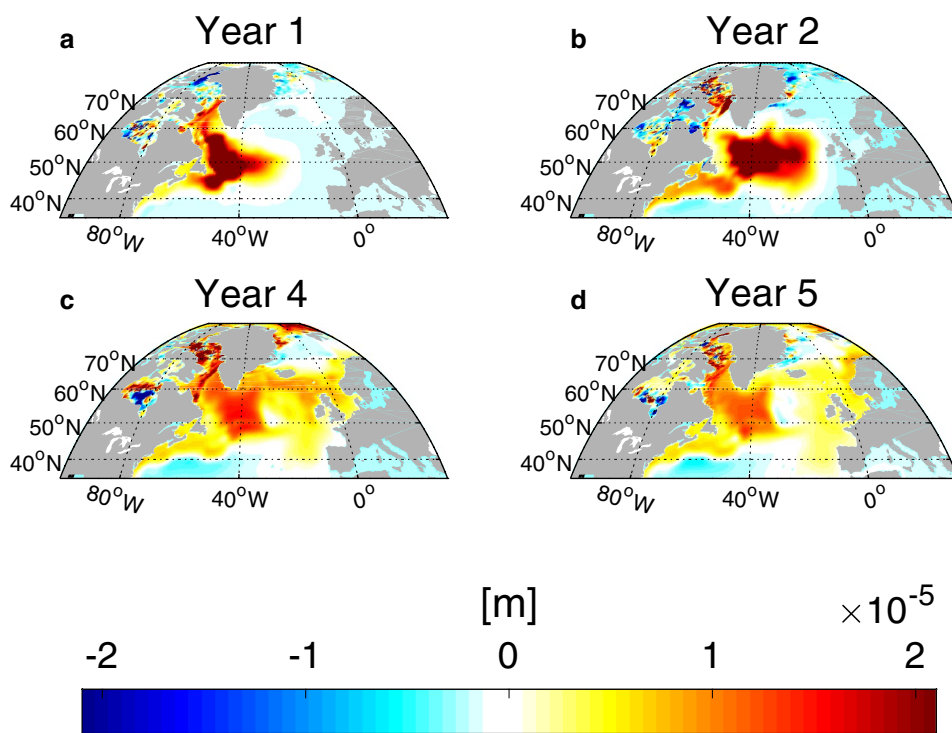

Fig. 4 Sea surface height anomaly [m], positive in red, averaged over: **a** Year 1; **b** Year 2; **c** Year 4; **d** Year 5 of the Labrador Sea freshening experiment (Pert1_LabSSS)

NEADW is a component of LNADW, which is more strongly stratified than the overlying Labrador Sea Water (LSW, σ_θ of 27.68–27.80 [kg m^{-3}], Yashayaev 2007; Rhein et al. 2015) but less stratified than the underlying Denmark Strait Overflow Water ($\sigma_\theta > 27.88$ [kg m^{-3}], (Yashayaev 2007; Rhein et al. 2015). Here we use these differences in stratification, represented by the primary component of planetary Ertel PV, to distinguish NEADW – a component of LNADW – from the overlying LSW (Figure S2 in the Supplementary Information) in the model.

The local maximum in the 26° N velocity anomaly between $\sigma_\theta = 27.81$ and $\sigma_\theta = 27.86$ [kg m^{-3}] motivates us to focus on

the meridional connectivity between the Labrador Sea and the subtropical AMOC in this LNADW layer. We see that the signal in the LNADW layer is communicated from the subpolar gyre to the low latitudes along the western boundary (Fig. 6). We thus define vertical sections within the North Atlantic at different locations along the boundary from Cape Farewell to 26°N, as illustrated in Fig. 6. We find that, after an initial adjustment, the response to Labrador Sea freshening becomes relatively coherent across a range of latitudes in the North Atlantic (Figs. 6 and 7).

We compare the meridional velocity anomalies at 26° N with the zonal velocity anomalies along a boundary section

Fig. 5 Overturning across 26°
N [m s^{-1}]: **a** climatology in
ECCO; **b** anomaly 5.5 years
after the Labrador SSS pertur-
bation shown in Fig. 2f (experi-
ment Pert1_LabSSS); **c** as in
b but enlarged and shown with
a different color scale to focus
on the transport anomaly in
the LNADW layer. Red (blue)
shading indicates northward
(southward) velocity. Superim-
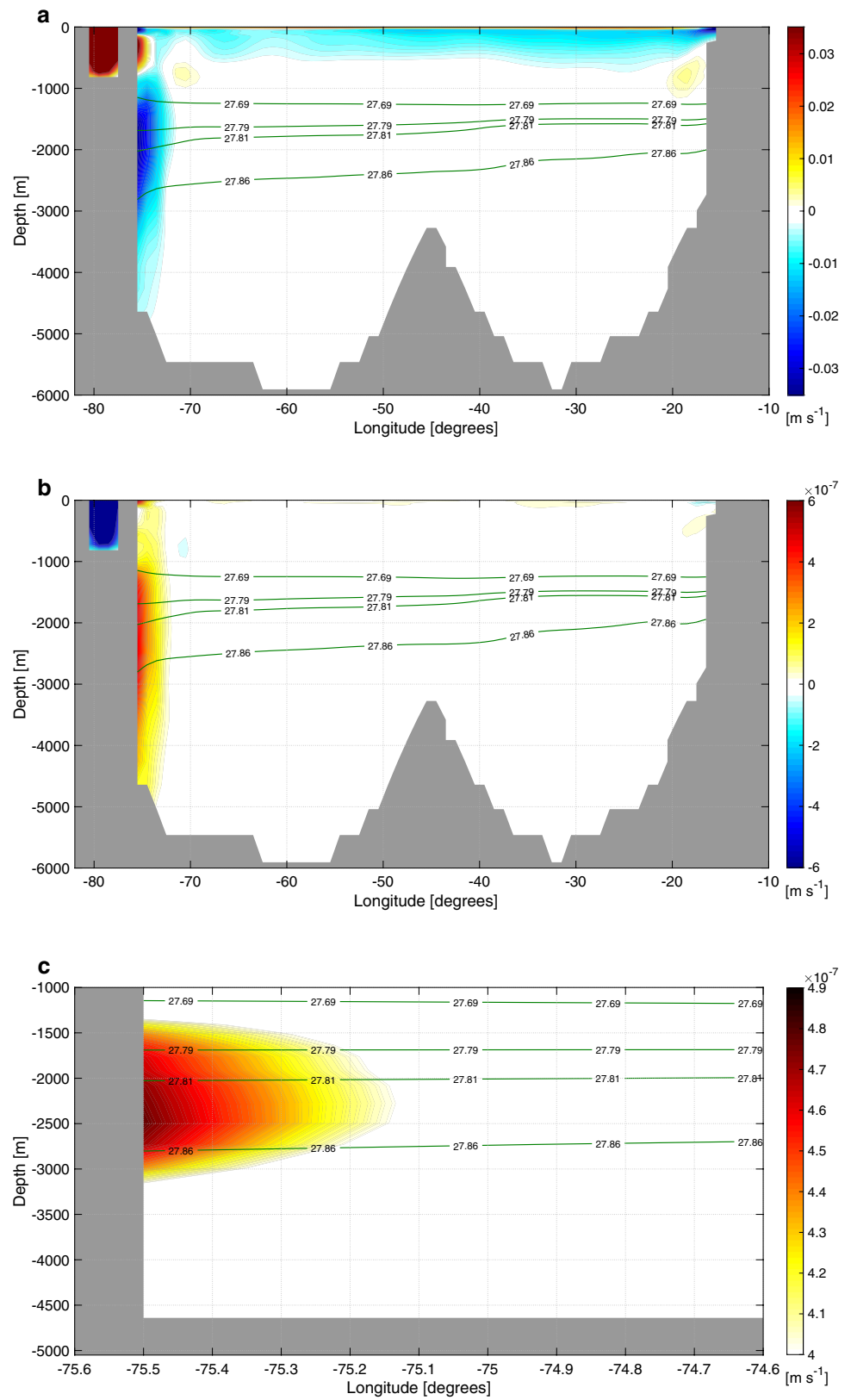posed green contours show σ_θ
potential density levels

Fig. 6 Meridional Velocity
Anomaly [m s^{-1}] in the σ_θ=
27.81–27.86 [kg m^{-3}] layer,
averaged over Year 4 of the
Labrador surface freshen-
ing perturbation experiment
(Pert1_LabSSS). Superimposed
are locations of the vertical sec-
tions in the model in dark green,
magenta, light green, and purple
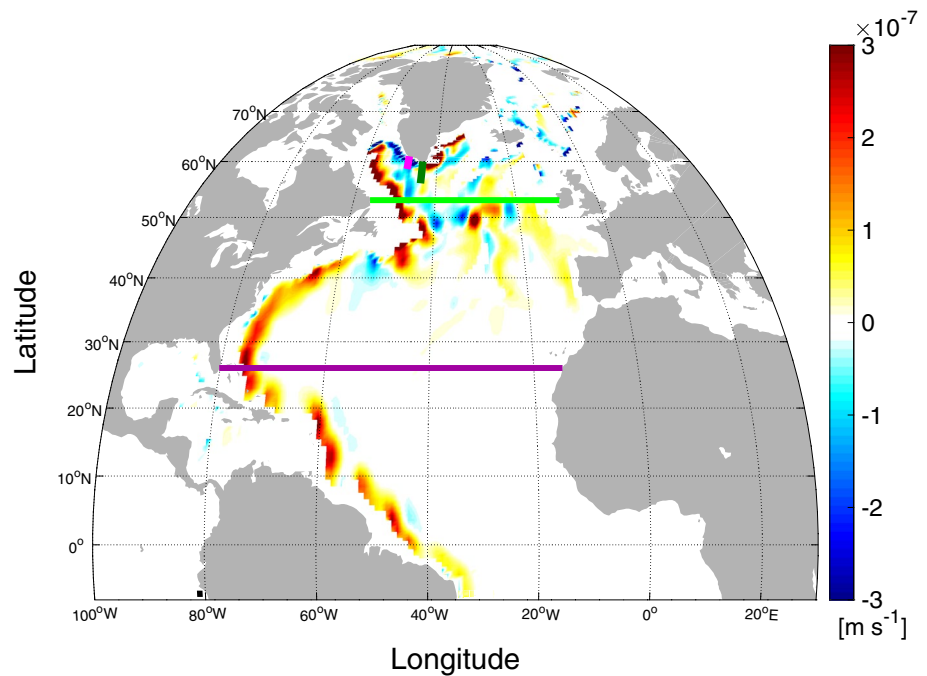
Fig. 7 LNADW transport
anomaly [Sv] across various
sections defined in the Labrador
SSS experiment (Pert1_Lab-
SSS). At the Cape Farewell and
Southern Greenland sections,
positive values indicate a
westward anomaly in response
to Labrador Sea freshening. At
all other sections positive values
indicate a southward anomaly.
The curves are color-coded
to match the section locations
showin in Fig. 6. Ticks along
the horizontal axis mark the
beginning of each year
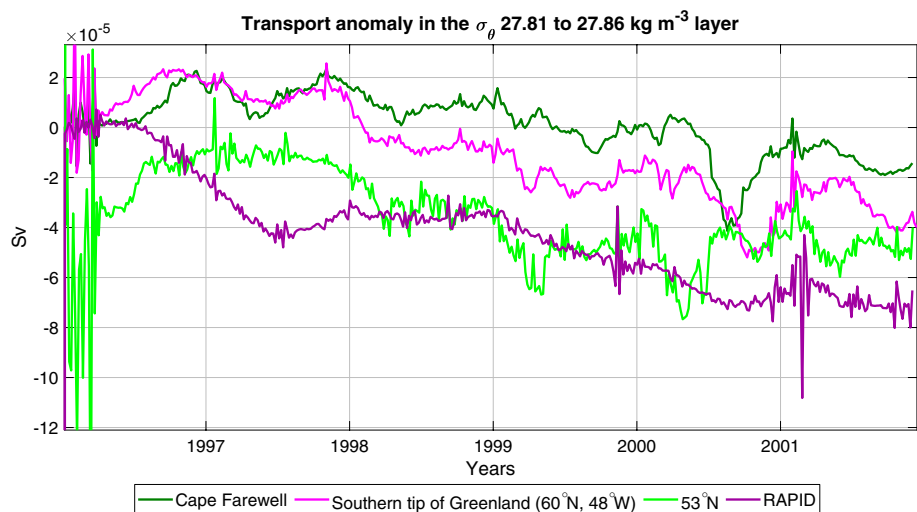
abutting Cape Farewell, as well as further west along the
southern coast of Greenland (Fig. 6). While at 26° N there
is a persistent subsurface maximum in the LNADW layer
(Fig. 8a, c), off Southern Greenland the velocity anomaly
is intensified above a depth of 1 km and decreases further
down in the water column (Fig. 8b, d). In September of
Year 5 in the Labrador Sea freshening experiment, a small
local maximum in the velocity anomaly emerges at depth
in the LNADW layer off Cape Farewell. However, overall,
the velocity anomaly in the subpolar gyre remains inten-
sified above 1000 m, unlike the response at 26° N. This
difference between the response off Cape Farewell and at
26° N can be understood in terms of the vertical profiles
of the subtropical and subpolar density anomalies (Fig. 9),

which correspond to anomalies in vertical shear of the hori-
zontal flow. Near southeastern Greenland, we see a very
pronounced negative anomaly in the in-situ density above
a depth of 1000 m (Fig. 9b). We find a small positive den-
sity anomaly along the boundary at greater depths. Hence,
in accordance with thermal wind balance, the anomaly in
the vertical shear in horizontal velocity off Cape Farewell
reverses sign at approximately 1 km. The maximum velocity
anomaly is thus found at depths above 1 km, but the velocity
anomaly throughout the water column can be attributed to
the upper ocean negative density anomaly.

Within the Northern Recirculation Gyre and further
south in the subtropics, we find that the negative in-situ
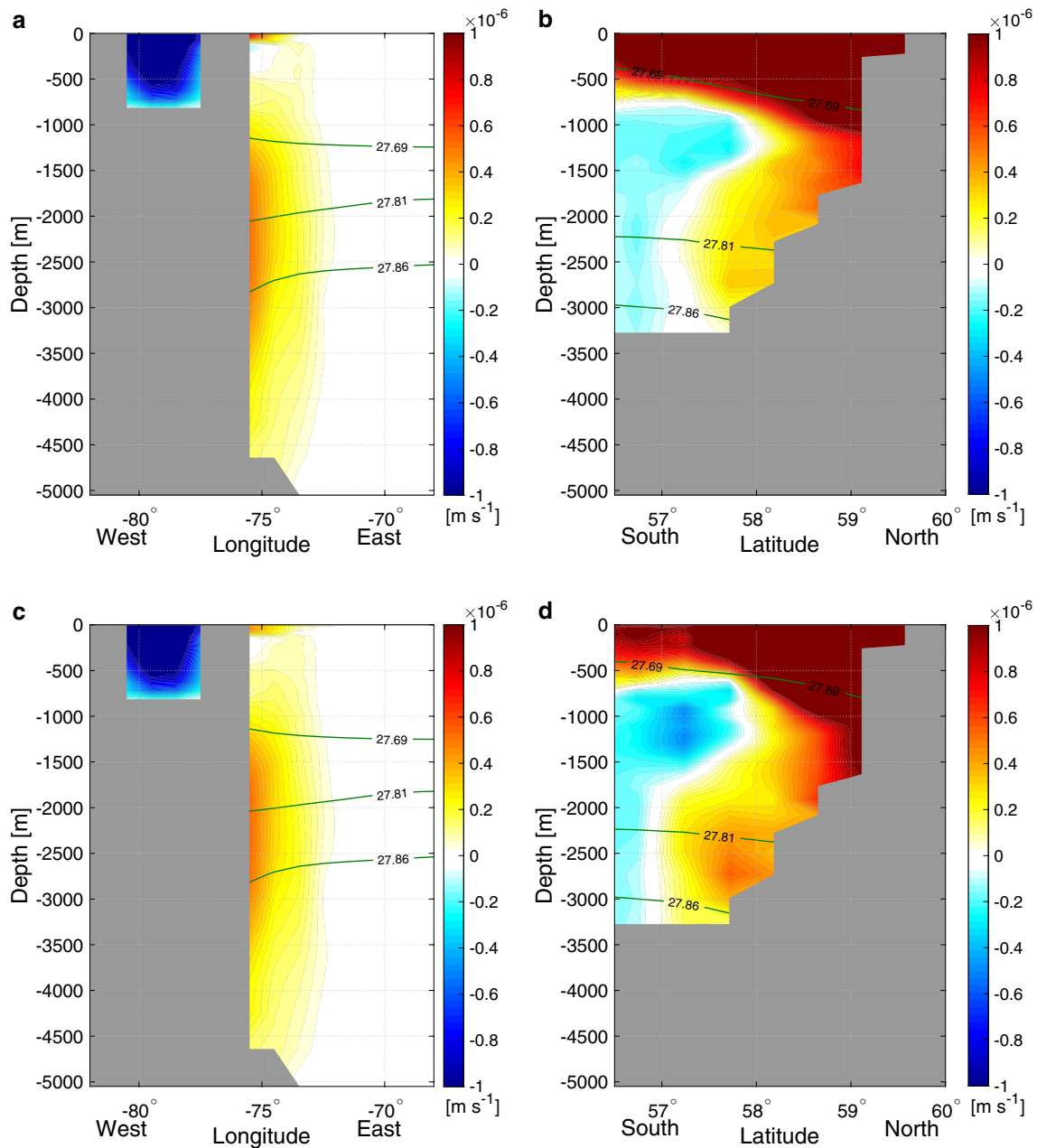density anomaly along the western boundary reaches down

Fig. 8 Comparison between the velocity anomaly [m s^{-1}] at 26° N (**a**, **c**) and the Cape Farewell boundary section (**b**, **d**) depicting the monthly-mean anomaly in June, 5.5 years (**a**, **b**), and in September, 5.75 years (**c**, **d**), after the original Labrador Sea surface salinity perturbation (experiment Pert1_LabSSS). See the map in Fig. 6 for the location of sections

to depths greater than 1000 m (Fig. 9a). The upper ocean signal originates in the subpolar gyre and is communicated along the western boundary. There is a small positive in-situ density anomaly along the boundary in the layers below $\sigma_\theta=$ 27.86 [kg m^{-3}]. Correspondingly, the anomalous vertical shear in horizontal velocity in the subtropics reverses sign between $\sigma_\theta=$ 27.81 and $\sigma_\theta=$ 27.86 [kg m^{-3}] (Fig. 9). Hence, according to thermal wind balance, the velocity response at RAPID reaches a maximum in the LNADW layer (Fig. 5b,

c). However, this subtropical response is still dominated by the negative density anomaly above 1 km (above the LSW layer). The difference in the vertical structure between the density anomalies in the subpolar and the subtropical gyre does not contradict the existence of meridional coherence in LNADW transport (Figs. 6 and 7). Our results, rather, suggest that the density anomaly above 1 km is what sustains the meridional coherence in the transport anomaly of the underlying LSW and LNADW layers.
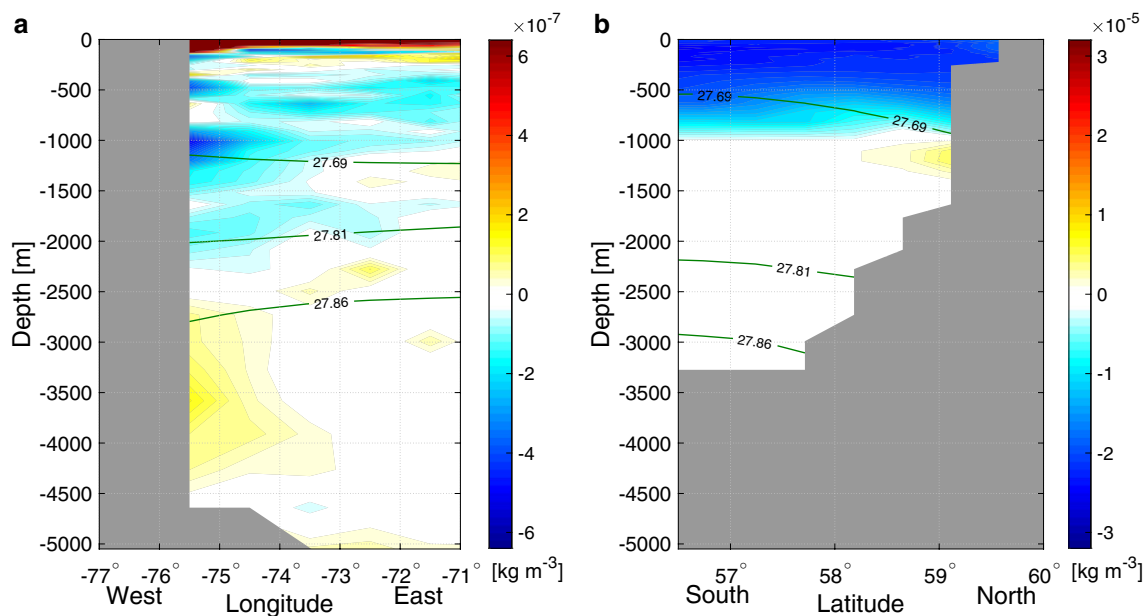
Fig. 9 In-situ Density Anomaly [kg m^{-3}] (color shading) and potential density [kg m^{-3}] (green contours) in Year 4 of the Labrador Sea freshening experiment Pert1_LabSSS at **a** 26° N, and **b** Southern Greenland (44°W). Notice that the colorscales in the two panels differ by a factor of 50. The Southern Greenland section is at 44°W, near Cape Farewell (See the sections shown in Fig. 6)

In order to illustrate the latter point, we perform an additional perturbation experiment, Pert3_1km26°N (Table 1 in Appendix). We sample the temperature and salinity anomalies averaged over Year 4 of the Labrador Sea freshening experiment. By that time, LNADW transport at 26°N has already responded. We select the anomalies only over a narrow subtropical latitude band (Fig. 10a, b) and only above a depth of 1 km. We apply these sampled anomalies as perturbations to temperature and salinity in a new experiment. Within days of this perturbation, we see a positive velocity anomaly in the DWBC at 26°N (Fig. 10c). This anomaly extends to depths of several kilometers and into the LNADW even though we have perturbed only the upper 1 km.

The results in this section motivate further analysis of the density response in the subpolar gyre, especially at depths shallower than 1000 m. In order to understand what governs the adjustment of the subpolar gyre, we perform an additional pair of experiments: a control simulation with a background passive tracer and a parallel experiment that is analogous to the original Labrador Sea SSS perturbation experiment. However, instead of modifying salinity, in this second experiment, we perturb the concentration of the passive tracer.

5 Adjustment in the subpolar gyre: background circulation and feedback

We conduct an experiment where we impose an initial condition anomaly in the surface concentration of a passive tracer (experiment Pert2_LabPtrac, see Table 1 in Appendix) relative to a control experiment with a passive tracer (Ctrl2_Ptrac, Table 1 in Appendix). The tracer perturbation has the same spatial pattern (Fig. 2f), sign, and magnitude as the SSS perturbation in our Labrador Sea freshening experiment Pert1_LabSSS. The passive tracer is furthermore processed by the same advection–diffusion and eddy parameterization schemes as salinity (and temperature) in the model. However, salinity feeds back on the ocean circulation, while the passive tracer does not. Comparing the results of the two simulations (Pert1_LabSSS and Pert2_LabPtrac) allows us to decompose density anomalies in the original Labrador Sea freshening experiment into a component due to transport by the background circulation/mixing and a remaining feedback component reflecting a dynamical response to freshening and a change in water mass transformation.

Four years after the passive tracer perturbation, we find a noticeable anomaly in its concentration within the LNADW layer of interest off the eastern coast of Greenland between Denmark Strait and Cape Farewell (Fig. 11). This is the main site where tracer perturbations originating
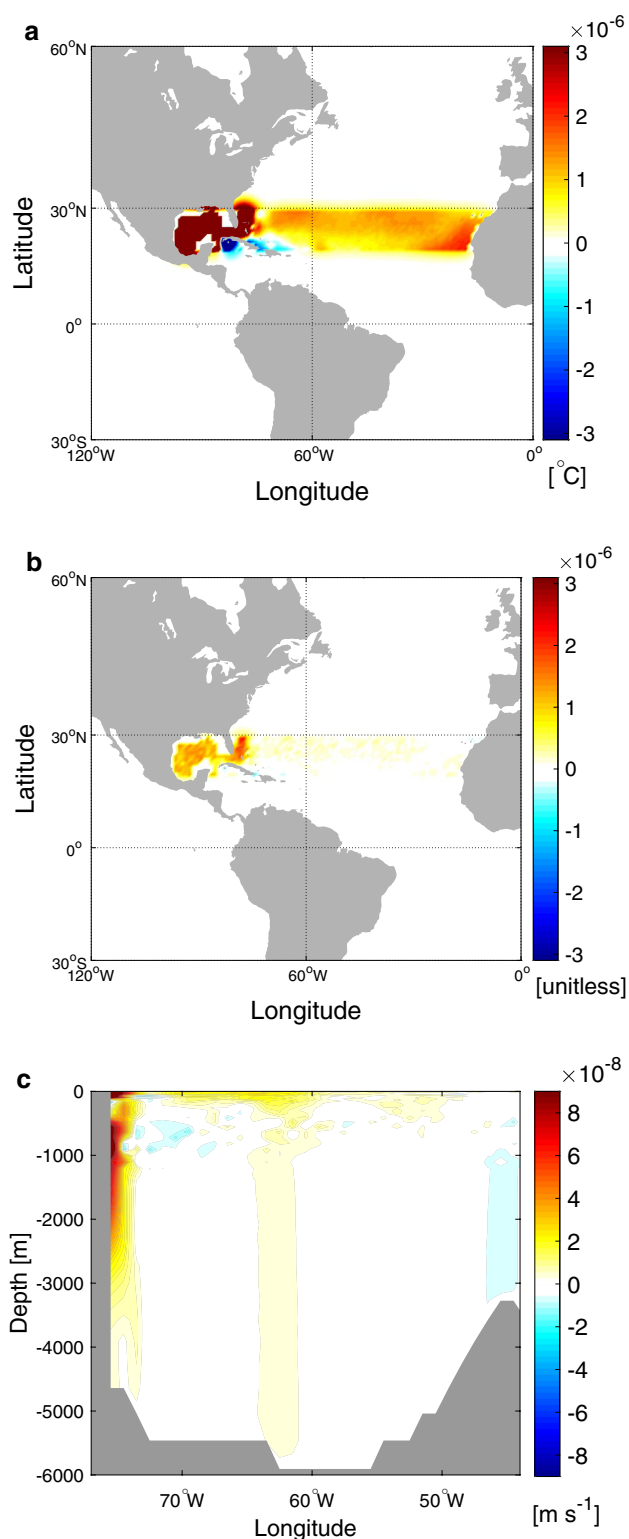
Fig. 10 SST (**a**) and SSS (**b**) anomalies from Year 4 of the freshening experiment (Pert1_LabSSS), sampled over a subtropical band. Temperature and salinity anomalies over 0–1 km within this subtropical band were applied as a perturbation in Experiment Pert3_1km26°N (Table 1). (**c**) The meridional velocity anomaly [m s^{-1}] 10 days after we perturb the upper 1 km temperature and salinity

at the surface of the Labrador Sea infiltrate the LNADW in ECCO on interannual timescales. The area immediately south of Denmark Strait is well known as a region where upper ocean water masses are entrained into the denser layers beneath (Falina et al. 2012; Harden et al. 2014). On interannual timescales, the passive tracer anomaly in the LNADW layer is then exported out of the Irminger Sea and propagates counterclockwise around the Labrador Sea (Figs. 11 and 12). In contrast, tracer uptake into the shallower LSW is governed by different mechanisms. The passive tracer signal efficiently infiltrates the LSW layer in the Labrador Sea with a particularly pronounced local penetration along the basin boundaries (Fig. 12), consistent with Desbruyeres et al. (2020).

We compare the original SSS perturbation and the passive tracer analogue experiment to explore the mechanisms that govern the negative trend (Fig. 7) in LNADW transport off the southern tip of Greenland in response to Labrador Sea freshening. In our analysis we treat the passive tracer as if it represented salinity that we then convert into a density anomaly. The latter is a counterfactual density anomaly that would exist in an ocean without any dynamical or air-sea feedback mechanisms. Subtracting this "passive" component of the potential density anomaly from the full potential density anomaly (σ_θ) field reveals the impact of feedback mechanisms. We find that the surface-intensified density anomaly in the subpolar gyre is *not* dominated by passive export of the original salinity perturbation from the Labrador Sea (Fig. 13a). The adjustment of the upper ocean circulation – and in particular, the NAC – exerts a strong positive feedback that amplifies the impact of the original Labrador Sea surface density anomalies by a factor greater than two (Fig. 13b). Note that Born et al. (2016) also suggest that anomalous flow dominates over passive advection of salinity anomalies in the North Atlantic subpolar gyre by a factor of two, but implies that these two sources of variability counteract each other. A major difference is that Born et al. (2016) focus primarily on negative feedback mechanisms related to the Irminger Current, while we highlight the positive feedback exerted by the NAC. In our analysis, the amplified upper ocean density anomalies act to slow down the subpolar gyre and decelerate the export of LNADW at depth.

In this study, we highlight that the NAC plays a key role in linking Labrador Sea surface anomalies to changes in the subtropical AMOC on fast timescales. In the following section, we piece together the full causal chain that explains the relationship between the results in Fig. 2. We show that in response to surface density anomalies in the western Labrador Sea, the NAC modifies overturning in the eastern subpolar gyre (where the OSNAP-EAST line is located), and this subsequently affects the DWBC at 26°N with a most pronounced velocity anomaly in LNADW. Finally, anomalies emerge in the ventilation of LSW and in the deep Lab Sea density, but

Fig. 11 Anomaly in the amount of passive tracer [m^3] integrated vertically over the LNADW layer ($\sigma_0 = 27.81-27.86$ [kg m^{-3}]), 4 years after the Labrador Sea passive tracer perturbation (experiment Pert2_LabPtrac)
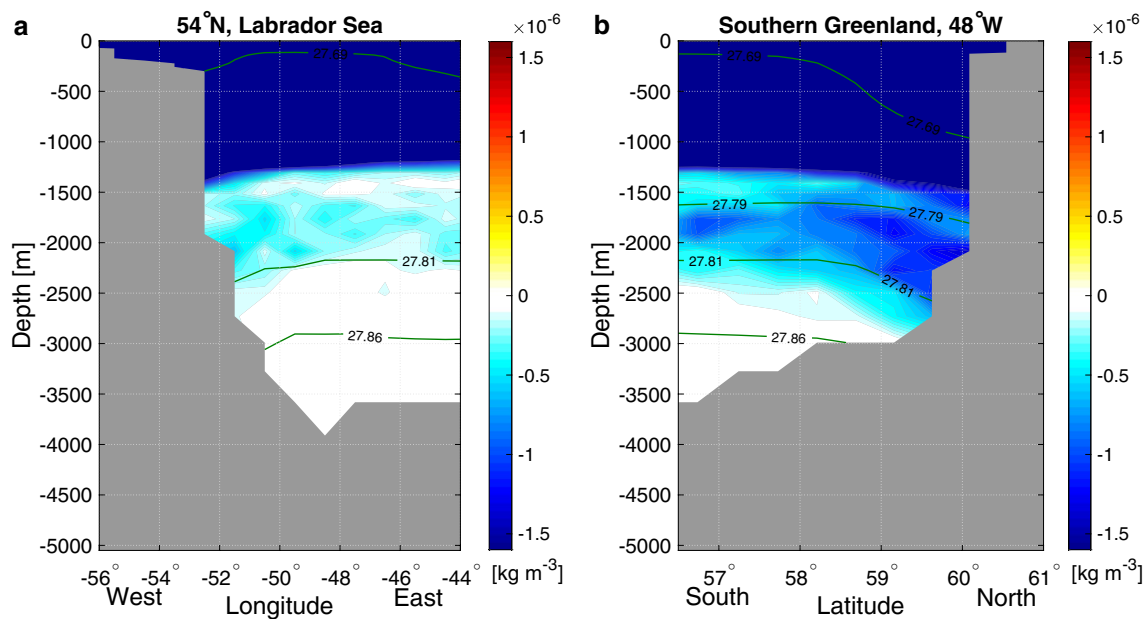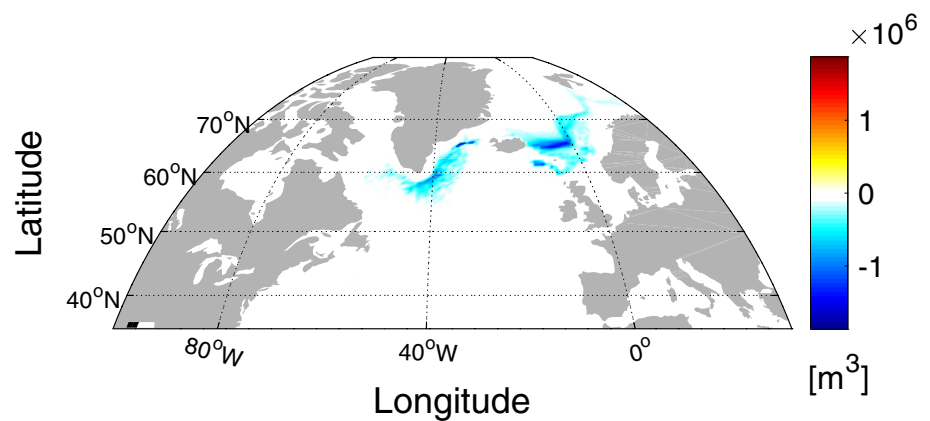

Fig. 12 Anomaly in the passive contribution to the density anomaly [kg m^{-3}] in Year 5 of experiment Pert2_LabPtrac. The passive tracer anomaly in experiment Pert2_LabPtrac is treated as if it had units of salinity, which is then converted to an equivalent locally-referenced density anomaly [kg m^{-3}]

these two components of the subpolar gyre system respond more slowly than the subtropical DWBC in our Labrador Sea freshening experiment.

## 6 Causal chain and the key role of the NAC

a. NAC weakening in Year 1

Our decomposition of the upper ocean density anomalies reveals that the NAC plays a key role both in transporting the imposed Labrador Sea salinity anomaly north-eastward (Fig. 13a) and in exerting a positive feedback on this original perturbation (Fig. 13b). Both components of the density anomaly in the upper subpolar gyre (the passive and the feedback component, Fig. 13) exhibit patterns that align with the NAC pathway.

The feedback component of the upper ocean potential density anomaly (Fig. 13b) is consistent with a slowdown of the NAC (Figure S3 in the Supplementary Information) in response to surface freshening in the western Labrador Sea. This slowdown reduces the inflow of warm, high salinity water from the subtropics (not shown) and leads to a further decrease in the upper ocean density across the subpolar gyre (Figs. 13b, 14b, and 15). Indeed, we see that in response to the Labrador Sea surface freshening, a positive sea-surface height (SSH) anomaly (Fig. 4a) reaches the mid-latitude "transition zone", and the meridional NAC transport across 45° N declines markedly (Figure S3 in the Supplementary

Fig. 13 Potential density (σ_θ) anomaly [kg m^{-3}] at a depth of 95 m, approximately 3 years (34 months) after the Labrador Sea surface salinity / passive tracer perturbation: **a** component due to transport of the original density perturbation (based on passive tracer experiment Pert2_LabPtrac); **b** feedback component due to redistribution of the background density as well as changes in water mass transformation (based on the difference between Pert1_LabSSS and Pert2_LabPtrac). Superimposed are contours of the sea-surface height (SSH) climatology in ECCO with higher (positive) climatological SSH in green, lower (negative) climatological SSH in purple, and zero contour in black. The contours are at intervals of 7 cm
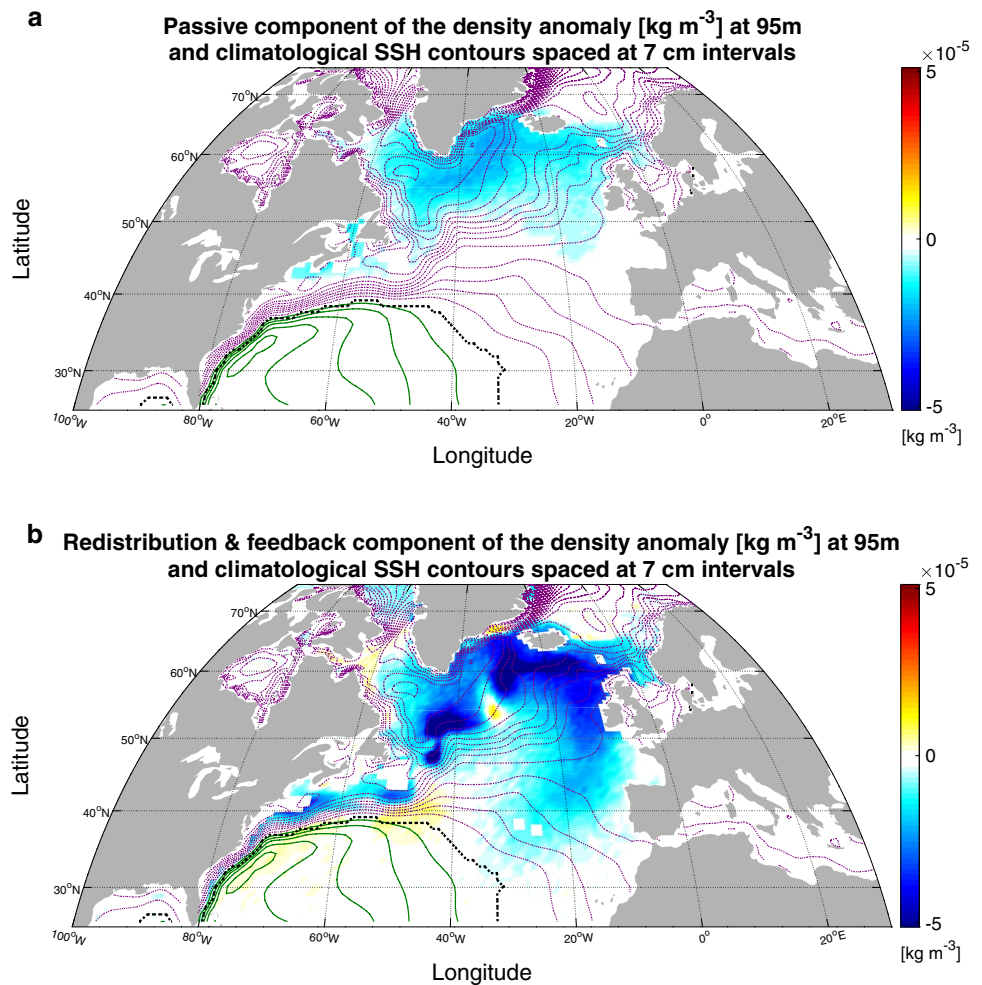

Information) before it recovers. This fast weakening, on a timescale shorter than a year, agrees with the prediction by the adjoint of the MITgcm (Fig. 2a), and is a first step in our causal chain linking the Labrador Sea with the subtropical LNADW transport (Fig. 16). The decline of the NAC can be attributed to changes in the geostrophic balance at 45°N (Figure S3 in the Supplementary Information) in response to the positive sea surface height anomaly originating in the Labrador Sea (see Fig. 4a). As the NAC slows down, there is a reduction in the surface heat loss to the north of Grand Banks because the air-sea heat exchange in this model is parameterized as a function of SST. This anomalous heat gain translates to an anomalous buoyancy flux into the ocean (Fig. 14a) during Year 1 of the freshening experiment.

The negative density anomaly in layers lighter than $\sigma_\theta = 27.69$ [kg m^{-3}] is rapidly communicated southward along the western boundary and affects the AMOC response at 26°N within a year after the Labrador Sea perturbation (Fig. 3). The negative density anomaly alters the zonal pressure gradient in

the underlying LSW and LNADW layers all the way to the subtropics and explains the fast response in the σ_θ range 27.81–.86 [kg m^{-3}] downstream of 53°N (Fig. 6). In the first year of the freshening experiment, this negative density anomaly signal at 26°N extends down to depths greater than 3 km and is well-confined to the western boundary (Fig. 17). By the second year of the freshening experiment, some of the negative density anomaly is stirred away from the boundary along isopycnals.

In addition to slowing down, the NAC also shifts southward (not shown), and this affects the transport of LNADW across the Mid-Atlantic Ridge through the Charlie Gibbs and Faraday Fracture zones (See Figure S4 in the Supplementary Information). The adjustment of the dense transport below the NAC gives rise to a local transport anomaly in the σ_θ range 27.81–.86 [kg m^{-3}]: a counterclockwise circulation whose northern and southern limbs align with the aforementioned fracture zones. This mechanism at depth complements the weakening of the NAC and leads to a further reduction of the southward LNADW export towards the subtropics.

Fig. 14 Anomaly in the surface-forced watermass transformation [kg m^{-2} s^{-1}] averaged over **a** the first and **b** the second year after the Labrador Sea surface salinity perturbation (experiment Pert1_LabSSS). These watermass transformation anomalies are due to surface heat flux anomalies, while the freshwater flux anomalies make a negligible contribution. Blue shading corresponds to regions of anomalous density loss (anomalous heat flux into the ocean), while red shading indicates areas of anomalous densification (anomalous heat flux out of the ocean)

Surface-forced watermass transformation anomaly Year 1

Surface-forced watermass transformation anomaly Year 2
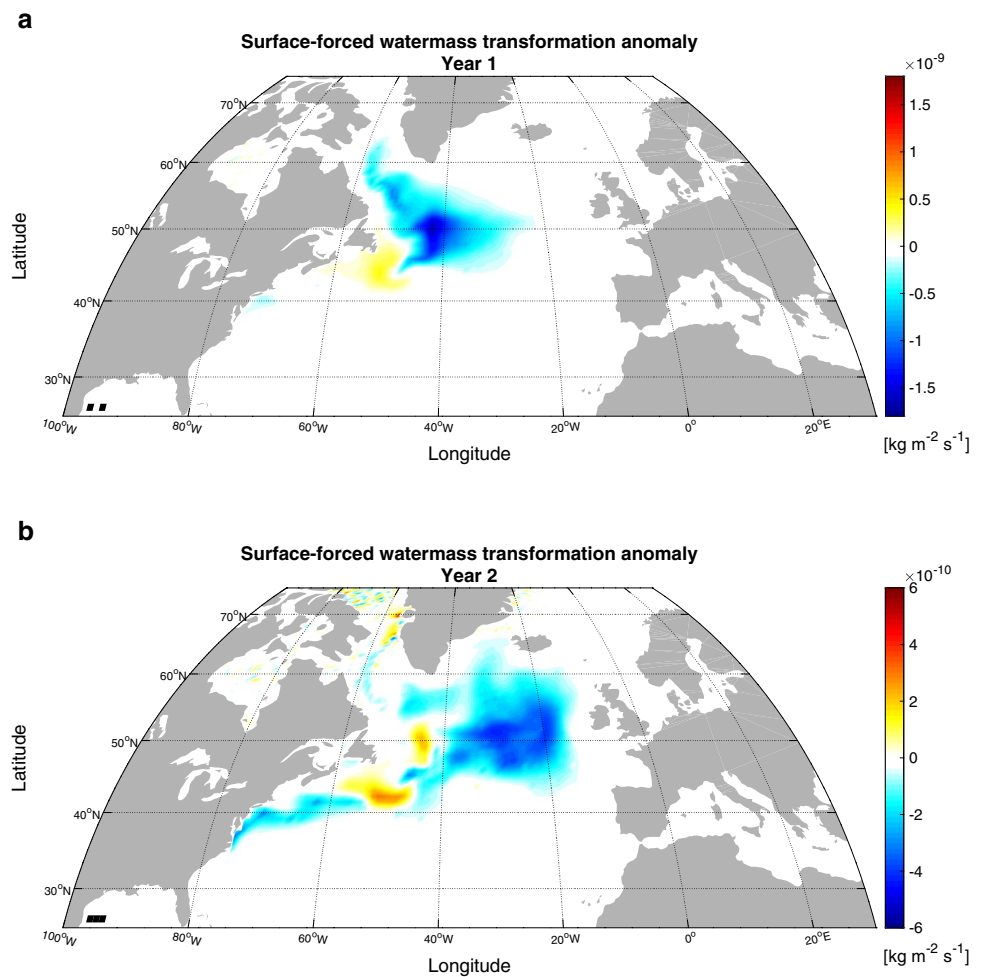
b. Water mass transformation changes in the Eastern Subpolar Gyre in Year 2

The slowdown of the NAC corresponds to anomalously weak northward transport of warm saline water (Lohman et al. 2009). As a result, a year after the adjustment of the NAC, we see a downstream negative anomaly of the surface spiciness relative to the control run (Fig. 21 in the Appendix) in the eastern subpolar gyre, consistent with the SST and SSS pattern in Lohman et al. (2009). Here spiciness represents the density-compensated temperature and salinity anomalies (Stipa 2002; Luo et al. 2005; Kilpatrick et al. 2011). We compute potential spiciness using the Huang et al. (2018) least-squares algorithm, appropriate for the modified UNESCO equation of state used in our model configuration (Jackett and McDougall 1995).

The negative SST anomaly in the Iceland Basin triggers a surface heat flux response (Fig. 14), that directly impacts the rate of surface-forced water mass transformation F [kg m^{-2} s^{-1}], (Figs. 14, 15a):

$$F = -\frac{\alpha Q}{C_p} - \frac{\beta(E-P)S}{1-S} \qquad (2)$$

where, following Speer and Tziperman (1992), Desbruyeres et al. (2019), and Petit et al. (2021), α and β are the thermal expansion and haline contraction coefficients, Q is the surface heat flux, C_p is the heat capacity of the uppermost layer, $(E-P)$ is the imbalance between evaporation and precipitation, and S is the SSS. In experiment Pert1_LabSSS, the response of F to Labrador Sea freshening is overwhelmingly dominated by the first term due to surface heat flux anomalies, while the contribution of freshwater fluxes is negligible (Fig. 15b). Remapping F into σ_θ coordinates allows us to compute the surface-forced overturning in density space following Desbruyeres et al. (2019).

Changes in surface water mass transformation over the Iceland Basin mark the second major step in our causal mechanism linking the Labrador Sea and the subtropics (Fig. 16). Even though we apply a freshening perturbation in the western Labrador Sea, the Year 2 surface buoyancy flux anomaly is largest in the eastern subpolar gyre, closer

Fig. 15 **a** Surface-forced water-mass transformation anomaly [10^{-4} Sv] in potential density space, averaged over the subpolar-gyre north of 45°N in different years following the Labrador Sea freshwater perturbation (experiment Pert1_ LabSSS). **b** Decomposition of the surface-forced water-mass transformation anomaly [10^{-4} Sv] in potential density space, averaged over the subpolar-gyre north of 45°N in Year 2 of the Labrador Sea freshwater pertur- bation (experiment Pert1_Lab- SSS). Transformation anomaly due to surface heat (orange) and freshwater fluxes (blue)
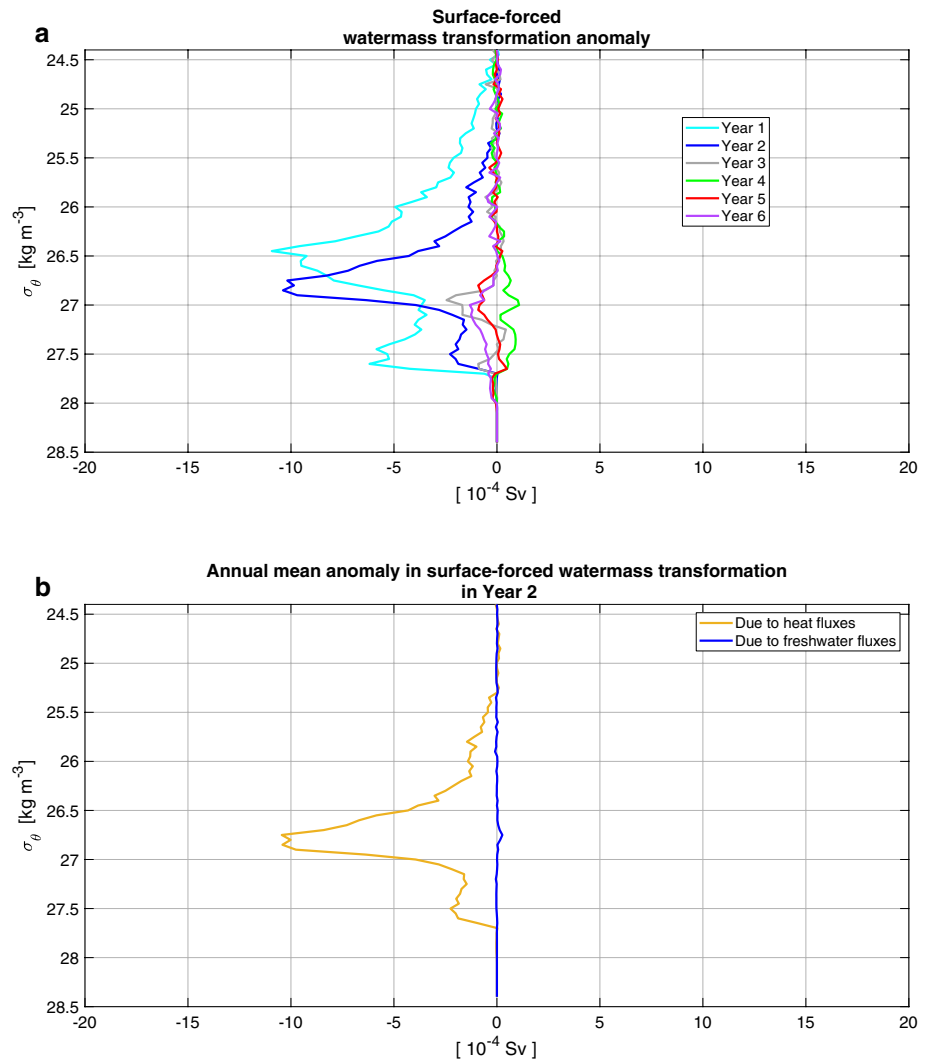
to the OSNAP-EAST array. We reiterate that the freshwater perturbation pattern in the Labrador Sea is applied to a region that represents an important source of SSS-driven historical AMOC variability over the recent decades (Fig. 2d, e and Kostov et al. 2021). This implies that typical SSS variability in the western Labrador Sea triggers changes in the water mass transformation further east (Fig. 14), and thus affects OSNAP-EAST overturning, (Fig. 3). This response of the sur- face heat fluxes is consistent with Desbruyeres et al. (2019) and Petit et al. (2020) who highlight the important role of the eastern subpolar gyre for the North Atlantic overturning in density coordinates.

The surface-forced water mass transformation anomaly in Year 2 is comparable in magnitude to the anomaly in Year 1 (Figs. 14 and 15), but decays in Year 3 (Fig. 15a) because the NAC exhibits a transient recovery (Figure S3 in the Sup- plementary Information), followed by a sustained but more gradual NAC decline. It is important to point out that the surface-forced transformation anomaly in the first two years

of the freshening experiment is confined to upper ocean layers lighter than $\sigma_\theta = 27.70$ [kg m^{-3}] – lighter than LSW and much lighter than LNADW. This once again highlights the impor- tant role of the upper ocean density anomalies for driving transport anomalies in the underlying layers. In other words, on this fast interannual timescale, the meridionally coherent LNADW transport anomaly is not due to a freshening of the LNADW layer itself, but is driven by the upper ocean.

c. Importance of the eastern subpolar gyre for connecting the Labrador Sea to the subtropics

The onset of the coherent LNADW response all the way from Southern Greenland to 26°N, and the evolution of the sub- tropical response, match the 3-to-4-year timescale on which the entire subpolar gyre slows down in response to Labrador Sea freshening, as reflected in the large-scale SSH anomaly in Year 4 of the experiment (Fig. 4c). Straneo (2006) and Born and Stocker (2014) decompose the velocity of the subpolar
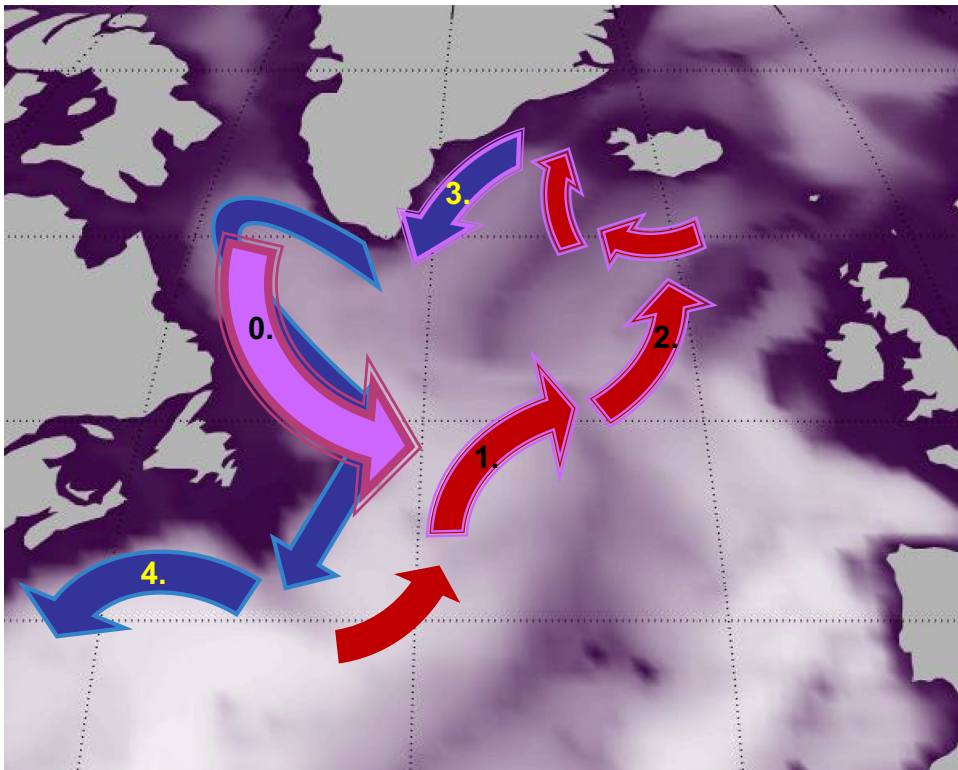
Fig. 16 Schematic showing the role of the NAC for meridional connectivity between the Western Labrador Sea and the subtropics in the LNADW layer. Buoyancy anomalies are advected out of the Labrador Sea (arrow 0) towards the Eastern Subpolar Gyre. In addition, buoyancy anomalies originating in the Labrador Sea lead to a weakening and a shift of the NAC (arrow 1). This triggers a coastally-trapped wave along the Western Boundary from the mid-latitudes to the subtropics and weakens the DWBC. The NAC response also affects the surface heat fluxes over the Iceland Basin and triggers changes in water mass transformation (arrow 2). This affects transport in the eastern subpolar gyre (arrow 3) and triggers a coastally-trapped wave from Southeast Greenland to the subtropics that leads to additional weakening of the DWBC. These NAC-mediated mechanisms slow down the DWBC, which leads to a positive density anomaly below 2 km in the Northern Recirculation and the Subtropical Gyre (arrow 4). As a result, the most pronounced slowdown in the subtropical DWBC is in the LNADW layer where the density anomaly reverses sign

gyre boundary currents into two components: (1) a baroclinic component that is in thermal wind balance with horizontal density gradients; and (2) a barotropic component that they attribute primarily to wind. Here we highlight the role of anomalous SSH gradients that are not generated by wind but by buoyancy anomalies and the mechanisms described in subsections a and b. Initially, the positive sea-surface height (SSH) anomaly, associated with a clockwise circulation anomaly, is confined to the narrow region where we apply the initial salinity perturbation (Figs. 2f and 4a). Both SSH and density anomalies affect the Montgomery potential (Roussenov et al. 2022) and sustain gyre circulation anomalies (Yeager et al.. 2021). The SSH anomaly, associated with a weakening of the subpolar gyre currents, gradually expands and reaches the eastern coast of Greenland within three to four years after the Labrador Sea freshening (Fig. 4b, c) during the period marked by reduced surface heat loss over the eastern subpolar gyre (Fig. 14). The weakening of both the eastern and the western subpolar gyre currents and the emergence of horizontal velocity anomalies near Southern Greenland (Fig. 4c) constitutes the third step in our causal chain (Fig. 16).

d. Connectivity along the western boundary

Once the circulation around Cape Farewell responds to the Labrador Sea freshening, how fast is the signal in LNADW transport propagated from Greenland southward to the subtropics? To address this question, we design an additional experiment., Pert4_CapeF (Table 1 in Appendix). We first sample the three-dimensional ocean temperature and salinity anomaly from surface to bottom off Cape Farewell from experiment Pert1_LabSSS, 5.5 years after the Labrador Sea freshening. By that time, the subtropical AMOC in the Labrador Sea freshening experiment has already exhibited a pronounced response. We then apply this regional anomaly as a new initial condition perturbation about the control run in order to set up "a clone" of the original Labrador Sea freshening experiment, Pert1_LabSSS. We thus test the sensitivity

Fig. 17 In-situ density anomaly
[kg m⁻³] (locally referenced) at
3 km, averaged over **a** months
6 to 12; **b**: months 36 to 48 of
the Labrador Sea freshening
experiment Pert1_LabSSS. c)
Climatology of in-situ density
[kg m⁻³] at 3 km in ECCO
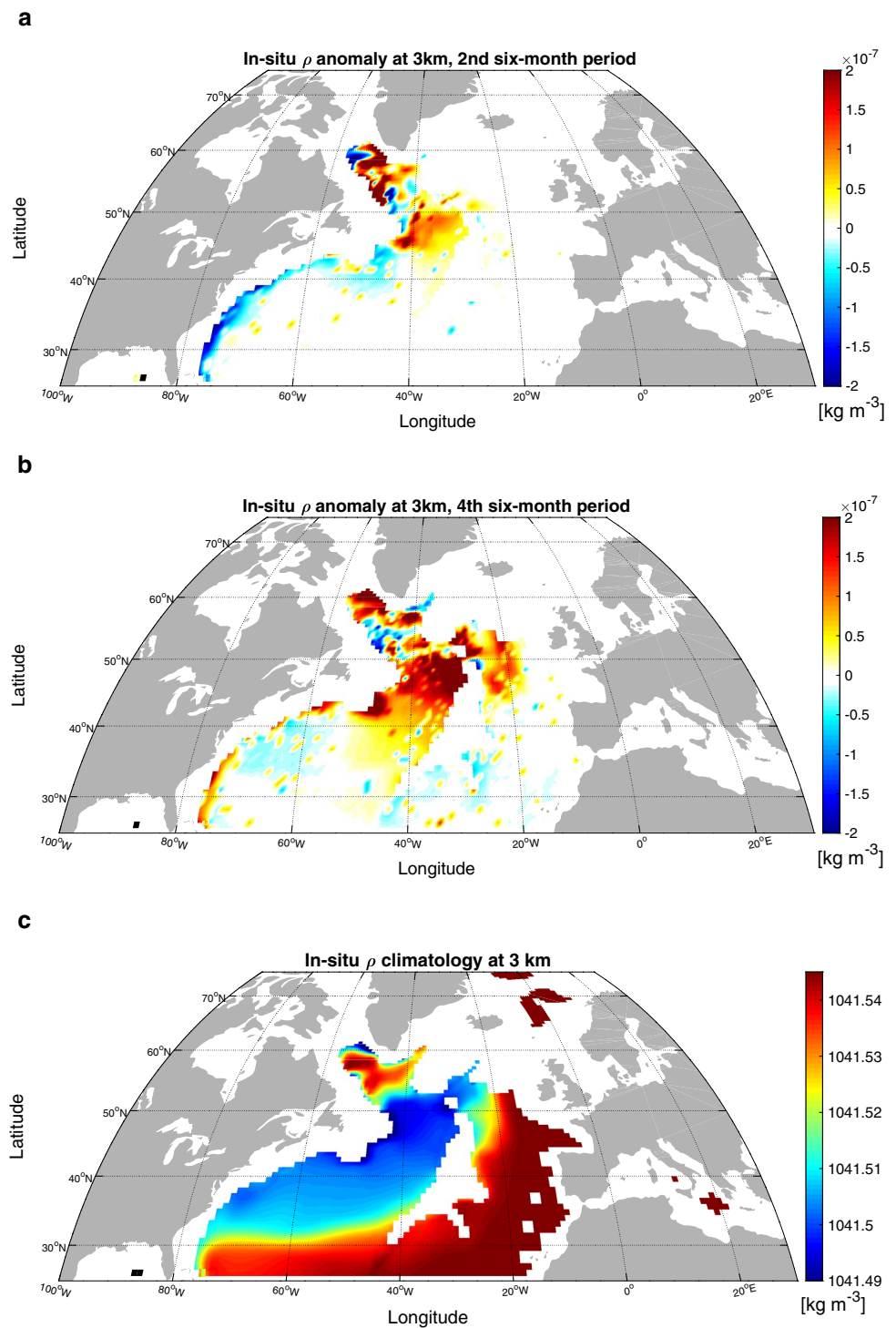
of downstream volume transport to density anomalies off the southern tip of Greenland.

We find that by applying a density anomaly in a small region off Cape Farewell, our "cloned" experiment (Pert4_CapeF) is able to reproduce a weakening of LNADW transport at 26° N within three months (Fig. 18). This implies that a coastally-trapped wave facilitates very fast connectivity

between Southern Greenland and 26° N along the western boundary. Therefore, the approximately four-year timescale of meridional connectivity between the Labrador Sea and 26° N is set by the gradual adjustment of the eastern subpolar gyre rather than by the southward propagation of the signal to the subtropics.

Fig. 18 Meridional velocity anomaly [m s^{-1}] at 26°N, three months after the Cape Farewell boundary perturbation (experiment Pert4_CapeF); Red/blue shading indicates northward/ southward velocity anomaly
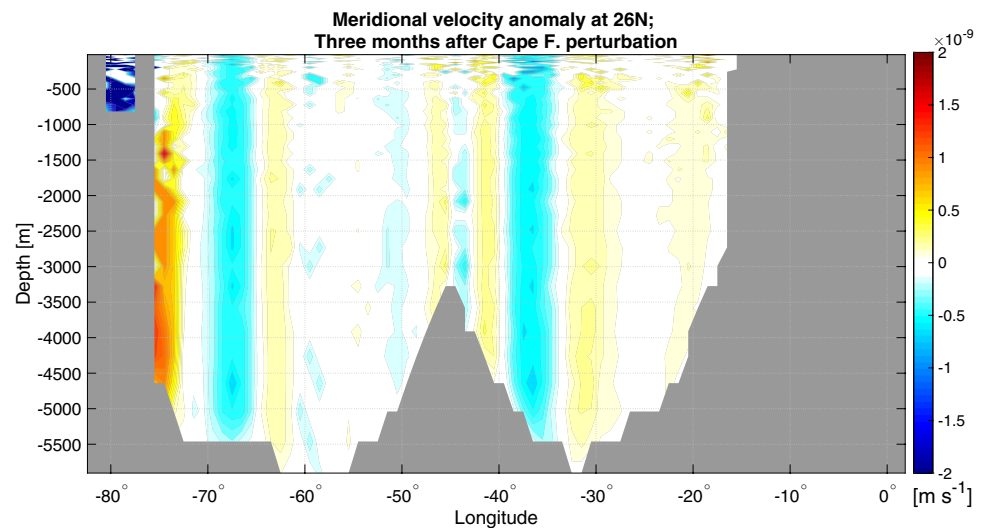
As discussed earlier, in the months after the NAC weakening, the negative density anomaly along the western boundary extends down to the densest layers (Fig. 17a). However, the northward velocity anomaly in the DWBC acts on the background meridional density gradients (Fig. 17c) and gradually gives rise to a small densification at layers deeper than $\sigma_\theta = 27.86$ [kg m^{-3}] (Fig. 17b and c). This produces the dipole density structure shown in Fig. 9a. In other words, the velocity anomaly pushes denser water northward at depth, redistributing the thickness of the densest layers. In our experiment, such densification does not emerge in the subtropical layers above 1 km because in this depth range the background density gradient is positive going from south to north (not shown). Hence, above 1 km, the northward velocity anomaly induces a negative density anomaly near the western boundary at these latitudes. The adjustment of the vertical density structure along the western boundary in the subtropics and the Northern Recirculation Gyre is the fourth step in our causal chain (Fig. 16). Because of this vertical dipole in the density anomaly, and in accordance with the thermal wind relation, the northward velocity anomaly at 26°N is in the LNADW layer (Fig. 5).

### e. Response of the LSW and deep Labrador Sea density

We now consider where ventilation of the LSW and the deep Labrador Sea density anomalies fit into our sequence of processes. In response to the freshwater perturbation, the volume of recently ventilated water (PV $< 4 \times 10^{-12}$ m^{-1} s^{-1}, following Zou and Lozier (2016)) remains approximately constant for the first three years of the experiment (Figure S5 a in the Supplementary Information). Then in Years 4 and 5, the volume of new LSW starts to decline in a more pronounced fashion (Figure S5a in the Supplementary Information). This does not appear to be related to background variability in LSW

production in ECCO, which serves as our control simulation (Figure S5b in the Supplementary Information) but is a lagged response to the freshwater perturbation. Note that this delayed response of LSW emerges after the subtropical DWBC has already declined.

We also examine the Labrador Sea density anomalies averaged between 1 km and 2.5 km, a metric suggested as a proxy for DWBC variability by Thornalley et al. (2018). Note that the deep Labrador Sea density anomaly is actually positive over the first 4 years of the experiment and switches sign only after the subtropical AMOC has already responded (Fig. 19). This sign reversal is due to a combination of factors: changes in the ventilation of LSW, and the penetration of negative density anomalies into LNADW constituents along the southeastern Greenland shelf, south of Denmark Strait (Figs. 11 and 12). The latter are gradually advected around Greenland on a timescale consistent with Menary et al. (2020), who show that overturning in the *dense* Labrador Sea layers (around $\sigma_\theta = 27.74$ kg m^{-3}) lags overturning anomalies at OSNAP-East by several years (compare with Figs. 3, 11, and 12). This lag is associated with the timescale of propagation along the East Greenland Irminger Current and the DWBC around Greenland.

Downwelling along the Labrador Sea boundary currents (Spall 2004; Straneo 2006; Born and Stocker 2014; Liu et al. 2022) is not an essential element in our fast connectivity mechanism. The deep penetration of density anomalies along the boundary is much weaker compared to the upper layer density anomaly and emerges late in our experiment (Figs. 9b, 11, and 12). In our study both LSW and deep Labrador density anomalies respond *after* the response of the eastern subpolar gyre and after the adjustment of the subtropical AMOC. Our results therefore suggest that neither LSW ventilation, nor dense overturning in the Labrador Sea, nor Labrador density anomalies between 1 and 2.5 km are drivers of

Fig. 19 Anomaly in the deep Labrador Sea density [kg m^{-3}] between 1 km and 2.5 km after the Jan. 1996 Labrador Sea surface freshening in experiment Pert1_LabSSS: annual-mean anomaly (diamonds) and 5-day mean anomaly smoothed with a 30-day running average (blue curve)
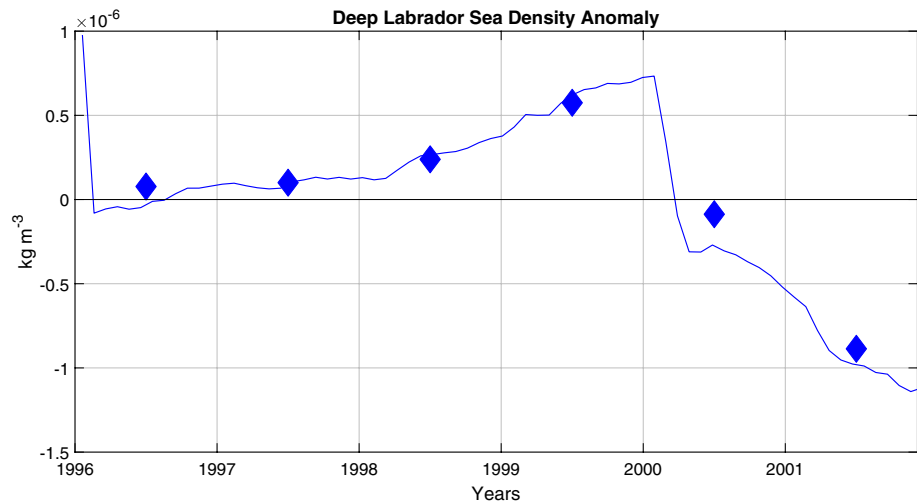
the fast connectivity mechanism that we have identified. Our analysis highlights the importance of the upper ocean layers lighter than LSW for communicating the subpolar signal to mid- and low latitudes on fast timescales, consistent with the findings of Roussenov et al. (2022).

f. Southward inter-gyre transport of the salinity anomalies

We furthermore consider the role of southward inter-gyre advection of salinity anomalies. Model simulations by Condron and Winsor (2011) suggest that surface salinity anomalies from the western subpolar gyre are exported to the subtropics on a timescale shorter than a decade. Similarly, we also find that 6 years after the Labrador Sea freshening, the SSS anomaly in the subpolar gyre interior is small, while a large part of the surface signal has shifted south-eastward towards lower latitudes (Fig. 22 in Appendix). This slow advection of the signal into the subtropics does not play a role in our fast north–south connectivity mechanism. Moreover, in contrast to Condron and Winsor (2011), we also see negative SSS anomalies along the Scottish and Norwegian shelves. These anomalies are not an essential element of the fast connectivity mechanism presented here.

7 The Western Labrador Sea and historical variability in the North Atlantic circulation

We have demonstrated a causal chain that links SSS anomalies in the Western Labrador Sea to meridionally coherent variability in LNADW transport and the subtropical AMOC. The adjustment of the NAC is an essential step in our causal chain. In this section, we look for evidence that such a sequence of mechanisms is indeed activated in the Atlantic Ocean. We therefore analyze historical variability in the ECCO v4 state

estimate (Forget et al. 2015a), which has been fitted to observations in a least squares sense.

We consider a normalized index for the geostrophic component of the meridional NAC transport across 45°N at depths above 500 m (Fig. S6 in the Supplementary Information) in ECCO. We sample the ECCO winter-time SSS and surface density anomalies at lead times of 1 year before periods of low and high NAC index, respectively (Fig. 23 in Appendix). We thus perform a low-minus-high composite of winter-time SSS and surface density anomalies over periods preceding positive and negative values of the NAC index (Fig. 23 in Appendix). The choice of a 1-year lead-time is motivated by the lagged response of the NAC at 45° N to surface density anomalies in the Western Labrador Sea (Fig. 2a and Figure S3 in the Supplementary Information). In our composite analysis, we define the winter season as January through April.

We find that, when performing a low-minus-high composite based on all winters over the 1992–2015 time period, a negative SSS anomaly (Fig. 23a in Appendix) and a negative surface density anomaly (Fig. 23b in Appendix) pattern emerge along the Western Boundary of the Labrador Sea. This suggests that freshening or reducing the surface density in the Western Labrador Sea can indeed drive negative anomalies in the NAC transport. However, this low-minus-high composite (Fig. 23 in Appendix) may capture multiple unrelated mechanisms that affect NAC variability including large-scale wind forcing (Hakkinen and Rhines 2009).

We thus consider three shorter periods marked by large fluctuations in the strength of the NAC (Figure S6 in the Supplementary Information and Fig. 20) and perform analogous low-minus-high composites. We find that periods marked by steep negative (positive) fluctuations in the strength of the NAC are preceded by wintertime surface freshening (salinification) in the Western Labrador Sea (Figure S6 in the Supplementary Information and Fig. 20). These SSS anomalies

Fig. 20 Low-minus-high composites of winter (January through April) SSS during periods leading up to large negative and large positive anomalies in the NAC transport (Figure S6 in the Supplementary Information) in the ECCO v4, release 3 state estimate. The composited fields lead the periods of large NAC excursions by 1 year, a choice motivated by the lagged response of the NAC to SSS in the Western Labrador Sea (Fig. 2a and Figure S3 in the Supplementary Information). See Fig. 24 (in Appendix) for the corresponding composites of winter-time surface density anomalies
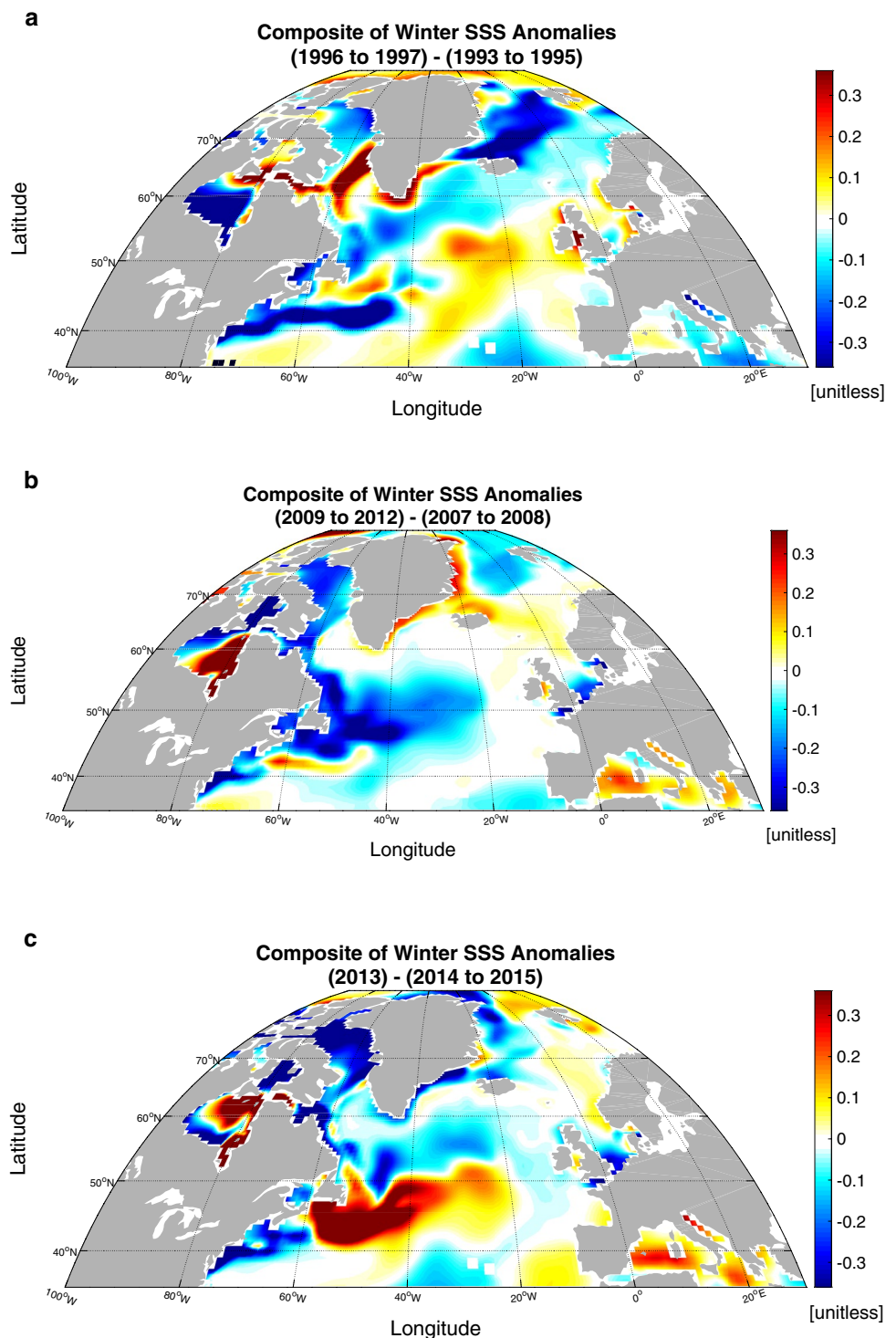
contribute to pronounced surface density anomalies (Fig. 24 in Appendix) along the basin boundary.

For example, the 2008–2011 weakening of the NAC is associated with a negative SSS anomaly along the western boundary of the Labrador Sea. The same period is marked by a step-decline in the subtropical AMOC (Smeed et al. 2014), which Kostov et al. (2021) reconstruct and attribute to surface density anomalies in the Western Labrador Sea. These results suggest that there are indeed historical periods when SSS anomalies along the boundary of the Labrador Sea have caused an adjustment of the NAC and triggered the causal chain that we have identified in our study.

8 Discussion and conclusion

We have identified two mechanisms that allow Labrador Sea density anomalies to impact the southward transport of LNADW and hence drive variability in the subtropical AMOC. The first mechanism involves the export of upper ocean buoyancy anomalies from the Labrador Sea by the background circulation: the Labrador Current and the NAC. These buoyancy anomalies spread throughout the upper layers of the subpolar gyre. Ultimately, the exported density anomalies reach the southeastern coast of Greenland between Denmark Strait and Cape Farewell, where the anomalies penetrate the LNADW layer in this region of enhanced entrainment. These LNADW density anomalies at depth have little dynamical impact on the subtropical overturning on fast timescales. They reach the deep Labrador Sea after the AMOC at 26° N has responded.

The second mechanism, which is dominant in our experiment, involves a geostrophic adjustment of the NAC, which amplifies the original density anomalies in the upper layers of the subpolar gyre. The buoyancy anomalies due to export from the Labrador Sea and those due to the NAC adjustment act in concert to modulate the entire subpolar gyre: a spin-up or a spin-down in the upper ocean that accelerates or decelerates the transport of LNADW constituents at depth. The North Atlantic Current (NAC) is an essential element in both the advection of buoyancy anomalies from the Labrador Sea and in the positive feedback that amplifies them. The background NAC transports buoyancy anomalies originating in the Labrador Sea towards the eastern coast of Greenland (Fig. 13a and the second arrow in Fig. 16). The NAC adjustment also plays a key role: a weakening of the current in response to Labrador Sea freshening leads to a reduction in the northward transport of high salinity water to the subpolar gyre and further decreases the surface salinity (Fig. 13b and the second arrow in Fig. 16) and the rate of water mass transformation in the subpolar gyre. As the NAC flowing over the CGFZ slows down, there is an intensification of the NAC over the Faraday Fracture Zone. In addition, the deep transport of LNADW across the MAR shifts southward in response to the NAC adjustment above.

The NAC weakening triggers a sequence of responses. First, a coastally-trapped wave communicates the upper ocean negative salinity anomaly from the region to the north of the Grand Banks to the subtropics. Then the eastern subpolar gyre gradually adjusts in response to Labrador Sea surface density anomalies over the course of several years. As the eastern subpolar gyre slowly adjusts, fast boundary-trapped waves continuously communicate the signal from Southern Greenland to the subtropics (Fig. 6). Across all latitudes, the resulting density anomaly along the western boundary is most pronounced in the layers lighter than LSW (Fig. 9). However, the meridional velocity anomaly in the subtropics is strongest in the LNADW layer (Fig. 5b, c), consistent with thermal wind balance. The LSW and the NEADW in the Labrador Sea itself also adjust in our freshening experiment, but the response of the deep Labrador Sea density emerges later compared to the subtropical AMOC response.

Our results recast the Zhang (2010) paradigm which proposes the existence of two regimes of north–south connectivity in the AMOC: fast (monthly) and slow (interannual). In our framework the interannual subpolar regime is dominated by *north-eastward* advection of density anomalies from the Labrador Sea along the NAC rather than direct southward advection along the deep western boundary current. We therefore propose that our mechanism may operate alongside the processes described in Zhang (2010).

Our results reconcile two seemingly conflicting paradigms regarding the north–south connectivity in the North Atlantic overturning: 1) Labrador Sea buoyancy anomalies impact subtropical AMOC variability (Eden and Willebrand 2001; Bailey et al. 2005; Getzlaff et al. 2005; Danabasoglu et al. 2012; Robson et al. 2014; Ortega et al. 2021); and (2) water mass transformation in the eastern subpolar gyre plays an overwhelmingly dominant role in AMOC variability in the subpolar regions (Lozier et al. 2019; Desbruyeres et al. 2019). We have explored a set of mechanisms that link the western Labrador Sea with meridionally coherent adjustment in the transport of LNADW constituents throughout the North Atlantic, from the south-eastern coast of Greenland to the subtropics.

The western part of the Labrador Sea is so efficient in driving overturning variability on fast timescales because the Labrador Current facilitates a fast export of density anomalies towards the so-called "mid-latitude transition zone" (Buckley and Marshall 2016) and the NAC. Our analysis highlights the importance of the NAC and its adjustment in the causal chain that facilitates meridional connectivity between the subpolar gyre and the subtropical AMOC on interannual timescales. Our results confirm previous studies suggesting that the so-called "mid-latitude transition zone" between the Labrador Current and the NAC is a pacemaker of Atlantic overturning variability (Buckley and Marshall 2016).

The NAC is known to play a major role in driving variability in the subpolar North Atlantic via advection-driven warming/cooling and salinification/freshening (Desbruyeres et al. 2021). For example, Desbruyeres et al. (2021) largely attribute the reversal of the observed North Atlantic cooling trend in 2016 to enhanced northeastward propagation of subtropical water masses. An interesting question that remains to be explored is whether this historical NAC shift, analyzed in Desbruyeres et al. (2021), has been triggered by surface density variability in the Labrador Sea following the mechanism described here. Our composite analysis based on the ECCO state estimate supports the hypothesis that the NAC strengthening in 2016 may indeed be a delayed response to SSS anomalies in the Western Labrador Sea (Fig. 20c).

Similarly, the extreme 2012–2016 freshening of the subpolar North Atlantic associated with a shift of the NAC (Penny Holliday et al. 2020) may also reflect some of the processes that we analyze in our study. In addition, Kostov et al. (2021) partially attribute the observed 2004–2012 step-decline in the AMOC at 26° N (Smeed et al. 2014) to surface density anomalies, most importantly SSS in the western Labrador Sea. Our results (Fig. 20) suggest that these mechanisms are indeed at play in the real ocean.

Our study has a number of limitations. Our analysis with an ocean-only model focuses only on the oceanic mechanisms linking the Labrador Sea, the eastern subpolar gyre, and the subtropics, and we do not fully explore the role of ocean–atmosphere coupling, which impacts AMOC variability on different timescales (Arthun et al. 2021). There is evidence that the North Atlantic Oscillation may play a role in an atmospheric teleconnection between the eastern and western parts of the subpolar gyre (Ortega et al. 2021). A further limitation of our approach is the use of a numerical model configuration which does not resolve eddies. It is known that the representation of mesoscale turbulence in models can affect the simulated NAC pathways and the propagation of tracers within and around the marginal seas of the subpolar North Atlantic (Böning et al. 2016). However, we expect the large scale dynamics to remain qualitatively similar across model configurations of different resolutions. Moreover, in our study the background ocean state is obtained from the ECCOv4 state estimate, which is fitted to observations, and hence represents the ocean realistically even in a nominal resolution of 1 degree (Forget et al. 2015a).

Finally, our results describe the AMOC adjustment in a regime linearized about a particular background state of the ocean. The analysis identifying the western boundary of the Labrador Sea as a driver of high-frequency variability is performed with the automatically generated adjoint of the MITgcm (Marotzke et al. 1999; Pillar et al. 2016; Smith and Heimbach 2019). The forward numerical experiments in this study involve deliberately small perturbations that do not significantly shift the system away from a linear regime of response. Hence, nonlinear effects due to convection, entrainment, and restratification of the mixed layer are beyond the scope of our analysis. In addition, linearizing the ocean physics about a different background state changes the magnitude and the time lag of the AMOC sensitivity to surface anomalies in the Labrador Sea (not shown), but we expect the causal chain that we outline to remain qualitatively similar. Our composite analysis of historical periods from the ECCO state estimate presented in this study and the skillful reconstruction of RAPID-AMOC variability in Kostov et al. (2021) suggest that insights from the linear regime remain valid in the context of recent historical variability.

In our experiments, Labrador Sea convection and deep density anomalies do not play a leading role on fast interannual timescales. However, Yeager et al. (2021) suggest that on longer timescales, the thickness of the LSW layer modulates the strength of the NAC and hence the subpolar overturning. The potentially important role of convection in the interior Labrador Sea for decadal AMOC variability (Oldenburg et al. 2021; Arthun et al. 2021) is beyond the scope of our study.

Despite these limitations, our study recovers the 3-to-4-year timescale of connectivity between the Labrador Sea and the subtropical AMOC (Zhang 2010) and identifies many of the important mechanisms and timescales at play. Establishing, confirming, and understanding the lagged relationship between observable *surface* density anomalies in the western Labrador Sea and the subtropical overturning implies that there is potential for predicting some of the low-frequency AMOC variability. This may pave the way for designing a more skillful AMOC prediction system.

Appendix

See Figs. 21, 22, 23, 24 and Table 1.

Fig. 21 Surface spice anomaly [kg m^{-3}] 2 years after the freshening of the Labrador Sea (Experiment Pert1_LabSSS)
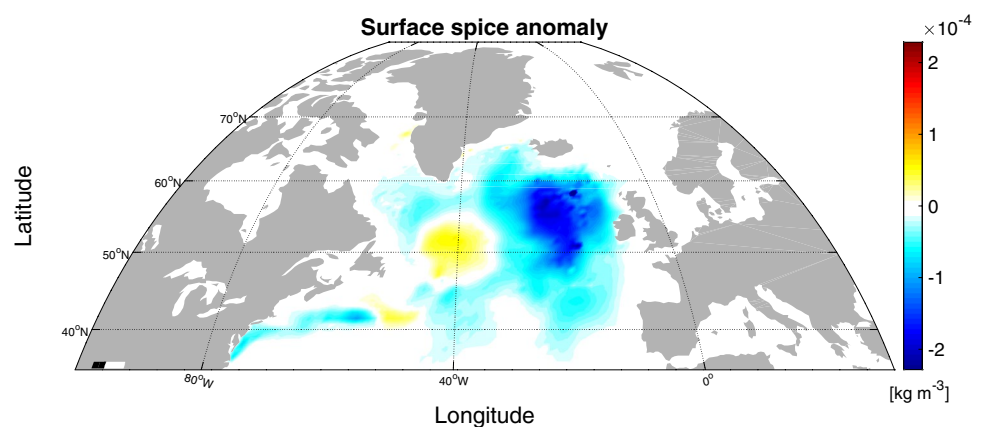
Fig. 22 SSS anomaly [unit-less] relative to the control simulation, 75 months after the Labrador Sea surface freshening perturbation (Experiment Pert1_LabSSS)
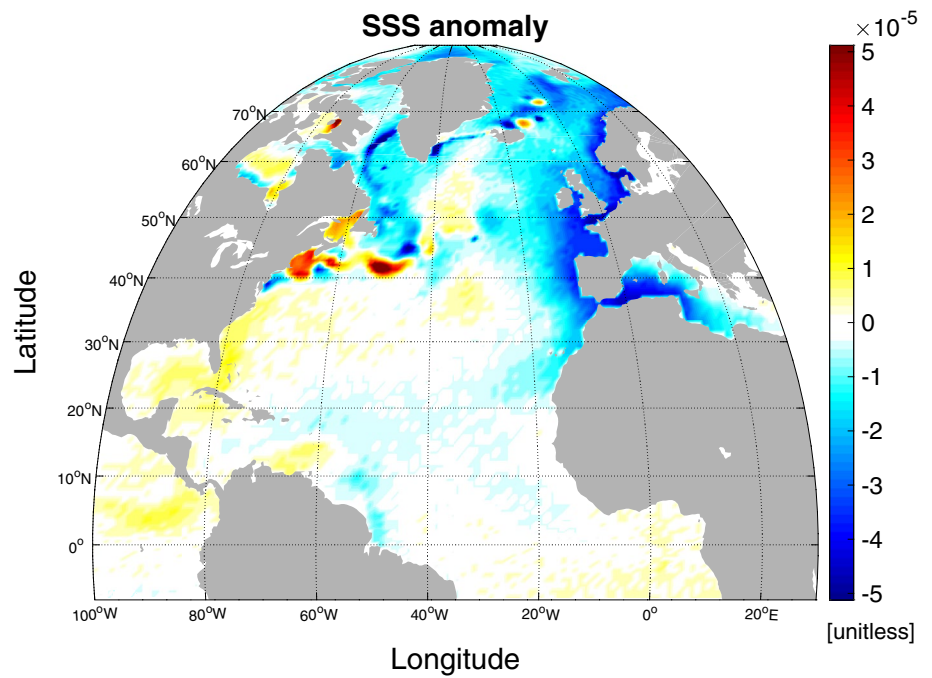

Fig. 23 Low-minus-high composites of winter (January through April) of **a** SSS [dimensionless] and **b** surface density anomalies [kg m^{-3}] during periods leading up to negative and positive anomalies in the NAC transport (Fig. S6 in the Supplementary Information) in the ECCO v4, release 3 state estimate. The composited fields lead the periods of large NAC excursions by 1 year, a choice motivated by the lagged response of the NAC to SSS in the Western Labrador Sea (Fig. 2a and Figure S3 in the Supplementary Information)
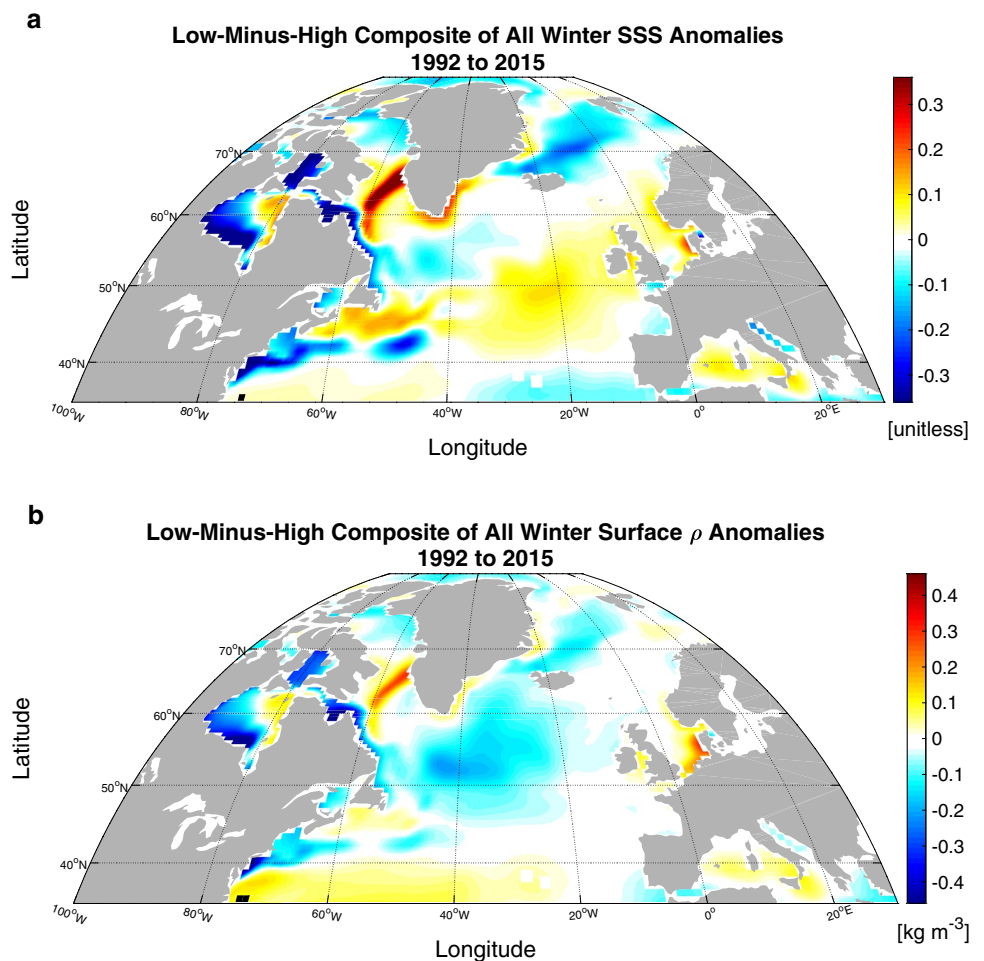
Fig. 24 Low-minus-high composites of winter (January through April) surface density anomalies [kg m^{-3}] during periods leading up to large negative and large positive anomalies in the NAC transport (Figure S6 in the Supplementary Information) in the ECCO v4, release 3 state estimate. The composited fields lead the periods of large NAC excursions by 1 year, a choice motivated by the lagged response of the NAC to SSS in the Western Labrador Sea (Fig. 2a and Figure S3 in the Supplementary Information)
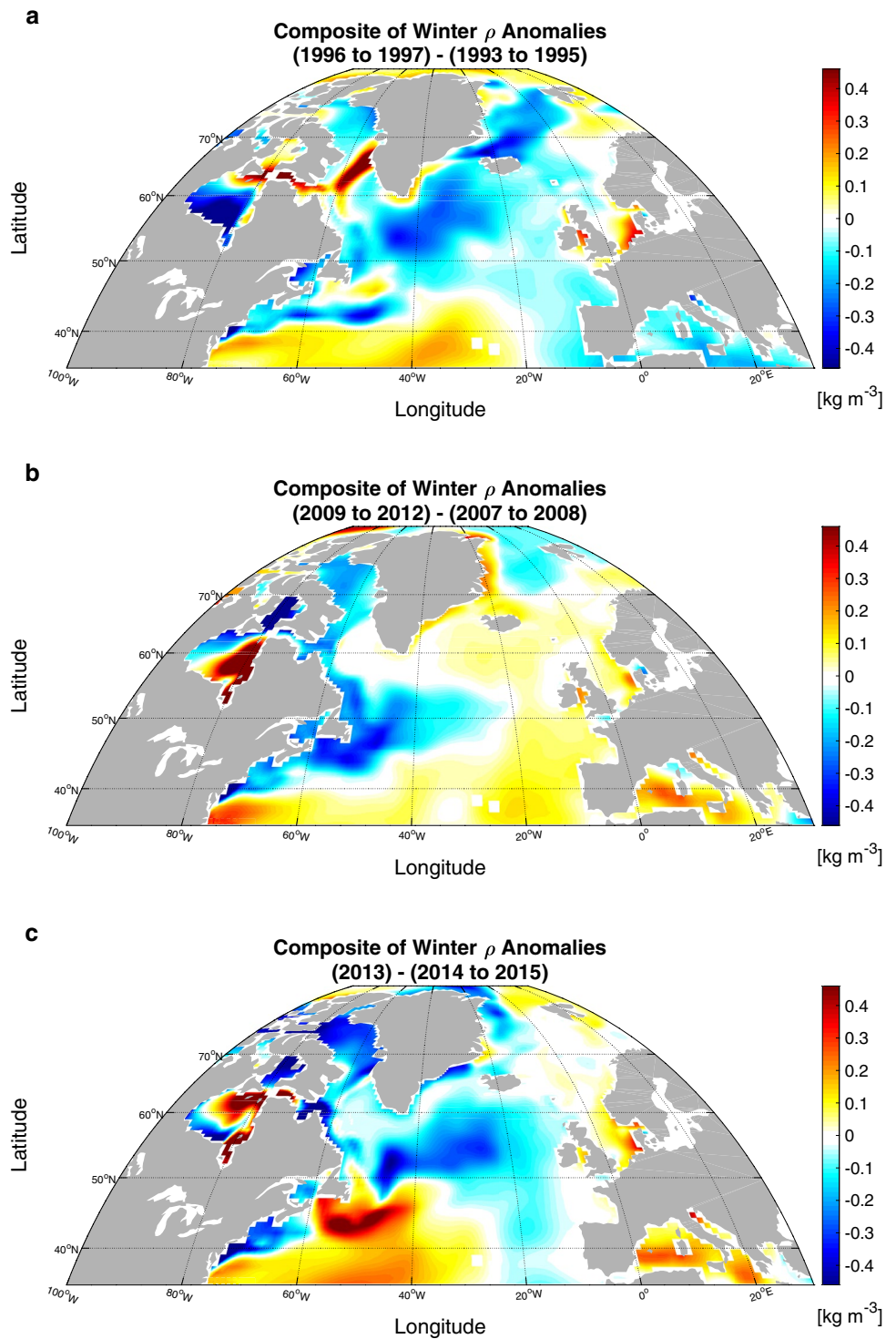
Table 1 Numerical experiments with the MITgcm and its adjoint

	Experiment	Type	Description
1	A1_NAC	Adjoint	Adjoint experiment calculating the sensitivity [Sv/ (psu sustained over 1 h)] of the winter NAC volume transport at 45°N to surface boundary conditions
2.[a]	A2_OSNAPE[a]	Adjoint	Adjoint experiment calculating the sensitivity of the spring OSNAP-East overturning to surface boundary conditions (from Kostov et al. 2021)[a]
3	A3_DWBC26	Adjoint	Adjoint experiment calculating the sensitivity of the winter-time southward DWBC transport at 26°N in the σ_θ range 27.81- 27.86 to surface boundary conditions. The DWBC cost function at 26°N was computed west of 70°W in a density layer corresponding to LNADW components
4.[a]	A4_AMOC26[a]	Adjoint	Adjoint experiment calculating the sensitivity of the winter RAPID-MOCHA overturning at 26°N to surface boundary conditions (from Kostov et al. 2021)[a]
5	Ctrl1_ECCO	Forward simulation	Re-run of the ECCOv4, r2 state estimate used as a background control simulation
6	Pert1_LabSSS	Forward perturbation	Perturbation of SSS in the Western Labrador Sea branched from Ctrl1_ECCO
7	Ctrl2_Ptrac	Forward simulation, passive tracer	Re-run of the ECCO state estimate with a background passive tracer
8	Pert2_LabPtrac	Forward perturbation, passive tracer	Passive tracer analogue of Pert1_LabSSS: perturbation of a passive tracer on the surface of the Western Labrador Sea with the same pattern and magnitude as the SSS perturbation in Pert1_LabSSS. The perturbation is applied relative to Ctrl2_Ptrac
9	Pert3_1km26°N	Forward perturbation	Perturbation of salinity and potential temperature over the upper 1 km in the subtropical North Atlantic using anomalies averaged over Year 4 of the Pert1_LabSSS. The perturbation is applied relative to Ctrl1_ECCO
10	Pert4_CapeF	Forward perturbation	Perturbation of salinity and potential temperature over the full water column along a boundary section off Cape Farewell. Imposed perturbations based on temperature and salinity anomalies sampled 5.5 years into Pert1_LabSSS. The perturbation is applied relative to Ctrl1_ECCO

All adjoint experiments represent a linearization of the MITgcm about historical periods from the ECCOv4, release 2, state estimate.

[a]Experiment from Kostov et al. (2021)

Declarations

References

Årthun M, Wills RCJ, Johnson HL, Chafik L, Langehaug HR (2021) Mechanisms of decadal North Atlantic climate variability and implications for the recent cold anomaly. J Clim 34(9):3421–3439. https://doi.org/10.1175/JCLI-D-20-0464.1

Bailey DA, Rhines PB, Häkkinen S (2005) Formation and pathways of North Atlantic Deep Water in a coupled ice–ocean model of

the Arctic-North Atlantic Oceans. Clim Dyn 25:497–516. https://doi.org/10.1007/s00382-005-0050-3

Böning CW, Scheinert M, Dengg J, Biastoch A, Funk A (2006) Decadal variability of subpolar gyre transport and its reverberation in the North Atlantic overturning. Geophys Res Lett 33(21):L21S01. https://doi.org/10.1029/2006GL026906

Böning C, Behrens E, Biastoch A et al (2016) Emerging impact of Greenland meltwater on deepwater formation in the North Atlantic Ocean. Nature Geosci 9:523–527. https://doi.org/10.1038/ngeo2740

Born A, Stocker TF (2014) Two stable equilibria of the Atlantic subpolar Gyre. J Phys Oceanogr 44(1):246–264. https://doi.org/10.1175/JPO-D-13-073.1%3e

Born A, Stocker TF, Sandø AB (2016) Transport of salt and freshwater in the Atlantic subpolar gyre. Ocean Dyn 66:1051–1064. https://doi.org/10.1007/s10236-016-0970-y

Buckley MW, Marshall J (2016) Observations, inferences, and mechanisms of the Atlantic meridional overturning circulation: a review. Rev Geophys. https://doi.org/10.1002/2015RG000493

Condron A, Winsor P (2011) A subtropical fate awaited freshwater discharged from glacial Lake Agassiz. Geophys Res Lett 38:L03705. https://doi.org/10.1029/2010GL046011

Danabasoglu G, Yeager SG, Kwon Y-O, Tribbia JJ, Phillips S, Hurrell JW (2012) Variability of the Atlantic meridional overturning circulation in CCSM4. J Clim 25:5153–5172. https://doi.org/10.1175/JCLI-D-11-00463.1

Desbruyères D, Mercier H, Maze G, Daniault N (2019) Surface predictor of overturning circulation and heat content change in the subpolar North Atlantic. Ocean Sci 15(3):809–817. https://doi.org/10.5194/os-15-809-2019

Desbruyères DG, Sinha B, McDonagh EL, Josey SA, Holliday NP, Smeed DA et al (2020) Importance of boundary processes for heat uptake in the subpolar North Atlantic. J Geophys Res 125:e2020JC016366. https://doi.org/10.1029/2020JC016366

Desbruyères D, Chafik L, Maze G (2021) A shift in the ocean circulation has warmed the subpolar North Atlantic Ocean since 2016. Commun Earth Environ 2:48. https://doi.org/10.1038/s43247-021-00120-y

Eden C, Willebrand J (2001) Mechanism of interannual to decadal variability of the North Atlantic circulation. J Clim 14:2266–2280. https://doi.org/10.1175/1520-0442(2001)014%3c2266:MOITDV%3e2.0.CO;2

Falina A, Sarafanov A, Mercier H, Lherminier P, Sokov A, Daniault N (2012) On the cascading of dense shelf waters in the Irminger sea. J Phys Oceanogr 42(12):2254–2267. https://doi.org/10.1175/JPO-D-12-012.1

Forget G, Campin JM, Heimbach P, Hill CN, Ponte RM, Wunsch C (2015a) ECCO version 4: an integrated framework for non-linear inverse modeling and global ocean state estimation. Geosci Model Dev 8:3071–3104. https://doi.org/10.5194/gmd-8-3071-2015

Forget G, Ferreira D, Liang X (2015b) On the observability of turbulent transport rates by Argo: supporting evidence from an inversion experiment. Ocean Sci 11:839–853. https://doi.org/10.5194/os-11-839-2015

Frajka-Williams E, Meinen CS, Johns WE, Smeed DA, Duchez A, Lawrence AJ, Cuthbertson DA, McCarthy GD, Bryden HL, Baringer MO, Moat BI, Rayner D (2016) Compensation between meridional flow components of the Atlantic MOC at 26° N. Ocean Sci 12:481–493. https://doi.org/10.5194/os-12-481-2016

Fukumori I, Wang O, Fenty I, Forget G, Heimbach P, Ponte RM (2017) ECCO Version 4 Release. http://hdl.handle.net/1721.1/110380

Fukumori I, Heimbach P, Ponte RM, Wunsch C (2018) A dynamically consistent, multivariable ocean climatology. Bull Am Meteorol Soc 99:2107–2128. https://doi.org/10.1175/BAMS-D-17-0213.1

Georgiou S, Ypma SL, Brüggemann N, Sayol J-M, Pietrzak JD, Katsman CA (2020) Pathways of the water masses exiting the Labrador Sea: the importance of boundary–interior exchanges. Ocean Model 150:101623. https://doi.org/10.1016/j.ocemod.2020.101623

Getzlaff J, Böning CW, Eden CB (2005) Signal propagation related to the North Atlantic overturning. Geophys Res Lett 32:L09602. https://doi.org/10.1029/2004GL021002

Giering R (2010)Transformation of algorithms in Fortran version 1.15 (TAF Version 1.9.70) (FastOpt, 2010)

Hakkinen S, Rhines PB (2009) Shifting surface currents in the northern North Atlantic Ocean. J Geophys Res 114:C04005. https://doi.org/10.1029/2008JC004883

Harden BE, Pickart RS, Renfrew IA (2014) Offshore transport of dense water from the east greenland shelf. J Phys Oceanogr 44(1):229–245. https://doi.org/10.1175/JPO-D-12-0218.1

Huang RX, Yu L-S, Zhou S-Q (2018) New definition of potential spicity by the least square method. J Geophys Res 123:7351–7365. https://doi.org/10.1029/2018JC014306

Jackett DR, Mcdougall TJ (1995) Minimal adjustment of hydrographic profiles to achieve static stability. J Atmos Ocean Technol 12(2):381–389. https://doi.org/10.1175/1520-0426(1995)012%3c0381:MAOHPT%3e2.0.CO;2

Jackson LC, Dubois C, Forget G, Haines K, Harrison M, Iovino D et al (2019) The mean state and variability of the North Atlantic circulation: a perspective from ocean reanalyses. J Geophys Res 124:9141–9170

Kilpatrick T, Schneider N, Di Lorenzo E (2011) Generation of low-frequency spiciness variability in the thermocline. J Phys Oceanogr 41(2):365–377. https://doi.org/10.1175/2010JPO4443.1

Kostov Y, Johnson HL, Marshall DP (2019) AMOC sensitivity to surface buoyancy fluxes: the role of air–sea feedback mechanisms. Clim Dyn 53:4521–4537. https://doi.org/10.1007/s00382-019-04802-4

Kostov Y, Johnson HL, Marshall DPD et al (2021) Distinct sources of interannual subtropical and subpolar Atlantic overturning variability. Nat Geosci 14:491–495. https://doi.org/10.1038/s41561-021-00759-4

Lherminier P, Mercier H, Gourcuff C, Alvarez M, Bacon S, Kermabon C (2007) Transports across the 2002 Greenland-Portugal Ovide section and comparison with 1997. J Geophys Res Oceans 112:C07003. https://doi.org/10.1029/2006JC003716

Li F, Lozier MS, Bacon S et al (2021) Subpolar North Atlantic western boundary density anomalies and the meridional overturning circulation. Nat Commun 12:3002. https://doi.org/10.1038/s41467-021-23350-2

Liu Y, Desbruyeres DG, Mercier H, Spall MA (2022) Observation-based estimates of Eulerian-mean boundary downwelling in the western subpolar North Atlantic. Geophys Res Lett 49:e2021GL097243. https://doi.org/10.1029/2021GL097243

Lohmann K, Drange H, Bentsen M (2009) Response of the North Atlantic subpolar gyre to persistent North Atlantic oscillation like forcing. Clim Dyn 32:273–285. https://doi.org/10.1007/s00382-008-0467-6

Lozier MS (2012) Overturning in the North Atlantic. Annu Rev Mar Sci 4:291–315. https://doi.org/10.1146/annurev-marine-120710-100740

Lozier MS et al (2019) A sea change in our view of overturning in the subpolar North Atlantic. Science 363(6426):516–521. https://doi.org/10.1126/science.aau6592

Luo Y, Rothstein LM, Zhang R-H, Busalacchi AJ (2005) On the connection between South Pacific subtropical spiciness anomalies and decadal equatorial variability in an ocean general circulation model. J Geophys Res 110:C10002. https://doi.org/10.1029/2004JC002655

MacGilchrist GA, Johnson HL, Marshall DP, Lique C, Thomas M, Jackson LC, Wood RA (2020) Locations and mechanisms of ocean ventilation in the high-latitude North Atlantic in an eddy-permitting ocean model. J Clim 33(23):10113–10131. https://doi.org/10.1175/JCLI-D-20-0191.1

Marotzke J, Giering R, Zhang KQ, Stammer D, Hill C, Lee T (1999) Construction of the adjoint MIT ocean general circulation model

and application to Atlantic heat transport sensitivity. J Geophys Res 104(C12):29529–29547. https://doi.org/10.1029/1999JC900236

Marshall J, Hill C, Perelman L, Adcroft A (1997) Hydrostatic, quasi-hydrostatic, and nonhydrostatic ocean modeling. J Geophys Res 102(C3):5733–5752. https://doi.org/10.1029/96JC02776

McCarthy G, Frajka-Williams E, Johns WE, Baringer MO, Meinen CS, Bryden HL, Rayner D, Duchez A, Roberts C, Cunningham SA (2012) Observed interannual variability of the Atlantic meridional overturning circulation at 26.5°N. Geophys Res Lett 39:L19609. https://doi.org/10.1029/2012GL052933

Menary MB, Jackson LC, Lozier MS (2020) Reconciling the relationship between the AMOC and Labrador Sea in OSNAP observations and climate models. Geophys Res Lett 47:e2020GL089793. https://doi.org/10.1029/2020GL089793

Oldenburg D, Wills RCJ, Armour KC, Thompson L, Jackson LC (2021) Mechanisms of low-frequency variability in North Atlantic Ocean heat transport and AMOC. J Clim 34(12):4733–4755. https://doi.org/10.1175/JCLI-D-20-0614.1

Ortega P, Robson JI, Menary M, Sutton RT, Blaker A, Germe A, Hirschi JJ-M, Sinha B, Hermanson L, Yeager S (2021) Labrador Sea subsurface density as a precursor of multidecadal variability in the North Atlantic: a multi-model study. Earth Syst Dyn 12:419–438. https://doi.org/10.5194/esd-12-419-2021

Penny Holliday N, Bersch M, Berx B, Chafik L, Cunningham S, Florindo-López C, Hátún H, Johns W, Josey SA, Larsen KMH, Mulet S, Oltmanns M, Reverdin G, Rossby T, Thierry V, Valdimarsson H, Yashayaev I (2020) Ocean circulation causes the largest freshening event for 120 years in eastern subpolar North Atlantic. Nat Commun 11(1):585. https://doi.org/10.1038/s41467-020-14474-y

Petit T, Lozier MS, Josey SA, Cunningham SA (2020) Atlantic deep water formation occurs primarily in the Iceland Basin and Irminger Sea by local buoyancy forcing. Geophys Res Lett 47:e2020GL091028. https://doi.org/10.1029/2020GL091028

Petit T, Lozier MS, Josey SA, Cunningham SA (2021) Role of air–sea fluxes and ocean surface density in the production of deep waters in the eastern subpolar gyre of the North Atlantic. Ocean Sci 17:1353–1365. https://doi.org/10.5194/os-17-1353-2021

Pillar H, Heimbach P, Johnson H, Marshall D (2016) Dynamical attribution of recent variability in Atlantic overturning. J Climate 29:3339–3352. https://doi.org/10.1175/JCLI-D-15-0727.1

Rhein M, Kieke D, Steinfeldt R (2015) Advection of North Atlantic Deep Water from the Labrador Sea to the southern hemisphere. J Geophys Res Oceans 120:2471–2487. https://doi.org/10.1002/2014JC010605

Robson J, Hodson D, Hawkins E et al (2014) Atlantic overturning in decline? Nature Geosci 7:2–3. https://doi.org/10.1038/ngeo2050

Rousseenov VM, Williams RG, Lozier MS, Holliday NP, Smith DM (2022) Historical reconstruction of subpolar North Atlantic

overturning and its relationship to density. J Geophys Res 127:32. https://doi.org/10.1029/2021JC017732

Smeed DA et al (2014) Observed decline of the Atlantic meridional overturning circulation 2004 to 2012. Ocean Sci 10(1):29–38. https://doi.org/10.5194/os-10-29-2014

Smith T, Heimbach P (2019) Atmospheric origins of variability in the South Atlantic meridional overturning circulation. J Clim 32(5):1483–1500. https://doi.org/10.1175/JCLI-D-18-0311.1

Spall MA (2004) Boundary currents and watermass transformation in marginal seas. J Phys Oceanogr 34(5):1197–1213. https://doi.org/10.1175/1520-0485(2004)034%3c1197:BCAWTI%3e2.0.CO;2

Speer K, Tziperman E (1992) Rates of water mass formation in the North Atlantic Ocean. J Phys Oceanogr 22:93–104. https://doi.org/10.1175/1520-0485(1992)022%3c0093:ROWMFI%3e2.0.CO;2

Stipa T (2002) Temperature as a passive isopycnal tracer in salty, spiceless oceans. Geophys Res Lett 29(20):1953. https://doi.org/10.1029/2001GL014532

Straneo F (2006) On the connection between dense water formation, overturning, and poleward heat transport in a convective basin. J Phys Oceanogr 36(9):1822–1840. https://doi.org/10.1175/JPO2932.1

Thornalley DJR, Oppo DW, Ortega P et al (2018) Anomalously weak Labrador Sea convection and Atlantic overturning during the past 150 years. Nature 556:227–230. https://doi.org/10.1038/s41586-018-0007-4

Yashayaev I (2007) Hydrographic changes in the Labrador Sea, 1960–2005. Prog Oceanogr 73(3–4):242–276. https://doi.org/10.1016/j.pocean.2007.04.015

Yeager S, Castruccio F, Chang P, Danabasoglu G, Maroon E, Small J, Wang H, Wu L, Zhang S (2021) An outsized role for the Labrador Sea in the multidecadal variability of the Atlantic overturning circulation. Sci Adv 7:eabh3592. https://doi.org/10.1126/sciadv.abh3592

Zhang R (2010) Latitudinal dependence of Atlantic meridional overturning circulation (AMOC) variations. Geophys Res Lett 37:L16703. https://doi.org/10.1029/2010GL044474

Zou S, Lozier MS (2016) Breaking the linkage between Labrador Sea Water production and its advective export to the subtropical gyre. J Phys Oceanogr 46:2169–2182. https://doi.org/10.1175/JPO-D-15-0210.1

Zou S, Lozier MS, Buckley M (2019) How is meridional coherence maintained in the lower limb of the Atlantic meridional overturning circulation? Geophys Res Lett 46:244–252. https://doi.org/10.1029/2018GL080958